Strong vorticity fluctuations and antiferromagnetic correlations in axisymmetric fluid equilibria

Peter B. Weichman
BAE Systems, Technology Solutions, 600 District Avenue, Burlington, Massachusetts 01803, USA

(Received 30 January 2019; published 28 May 2019)

The macroscale structure and microscale fluctuation statistics of late-time asymptotic steady-state flows in cylindrical geometries is studied using the methods of equilibrium statistical mechanics. The axisymmetric assumption permits an effective two-dimensional (2D) description in terms of the (toroidal) flow field σ about the cylinder axis and the vorticity field ξ that generates mixing within the (poloidal) planes of fixed azimuth. As for a number of other 2D fluid systems, extending the classic 2D Euler equation, the flow is constrained by an infinite number of conservation laws, beyond the usual kinetic energy and angular momentum. All must be accounted for in a consistent equilibrium description. It is shown that the most directly observable impact of the conservation laws is on σ, which displays interesting large-scale radius-dependent flow structure. However, unlike in some previous treatments, we find that the thermodynamic temperature is always positive. As a consequence, except for an infinitesimal boundary layer that maintains the correct (conserved) value of the overall poloidal circulation, the impact on ξ resides in the statistics of the strongly fluctuating, fine-scale mixing, where it is sensitive to "antiferromagnetic" microscale correlations that help maintain the analog of local charge neutrality. The poloidal flow is macroscopically featureless, displaying no large-scale circulating jet- or eddylike features (which typically emerge as negative temperature states in analogous Euler and quasigeostrophic equilibria).

DOI: 10.1103/PhysRevFluids.4.054703

I. INTRODUCTION

The modern era of exact statistical treatments of the late-time steady states of two-dimensional (2D) fluid flows, properly accounting for the infinite number of conserved integrals of the motion, began with the Miller–Robert–Sommeria (MRS) theory of the 2D Euler equation [1–4], generalizing earlier approximate treatments going all the way back to the seminal work of Onsager [5], and progressing through the Kraichnan energy–enstrophy theory [6], various formulations of the point vortex problem (see, e.g., Refs. [7,8]), and extensions to the quasigeostrophic equations [9–11]. Since then, the theory has been applied to significantly more complex systems, containing multiple interacting fields (in contrast to the Euler equation, which reduces to a single scalar equation for the vorticity), but still possessing an infinite number of conserved integrals [12]. These include magnetohydrodynamic equilibria [13–15], the shallow water equations [16–18], as well as numerous other geophysical applications [19].

Here we return to the example of 3D axisymmetric flows, refining and substantially extending a theory presented in Ref. [20] (as well as related earlier work relying on various simplifying assumptions [21,22]). These flows, sketched in Fig. 1, are interesting because they allow constrained interaction between circulation about the cylinder axis (toroidal flow) and circulation within any given fixed 2D azimuth plane containing that axis (poloidal flow). A novel aspect of this system, making it substantially different from the classic case of the Euler equation, is that although the key 2D dynamics occur in the "poloidal plane," the vorticity field ξ in that plane is not conserved by

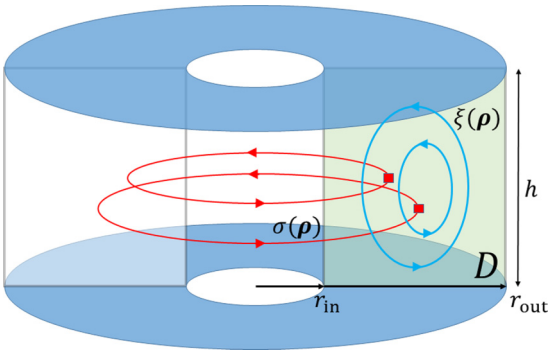

FIG. 1. Axisymmetric flow geometry. The pattern of flows is assumed to be invariant under rotation about the cylinder axis, and hence may be fully specified by the toroidal flow field σ about the axis [Eq. (7)], and poloidal vorticity field ξ [Eq. (9)] within any 2D radial plane D.

the flow. Rather, it is the toroidal field σ that is passively advected, and is then constrained by an infinite number of conserved integrals. It is therefore the indirect effects of σ-conservation that must feed back on ξ to generate any interesting equilibrium poloidal flow structure. One consequence is that, due to the comparatively weak constraints on ξ, the equilibrium state is strongly fluctuating and only positive temperature equilibria are permitted. This is in contrast to the Euler case in which the direct constraints on the vorticity field strongly suppress fluctuations, the equilibria may derived from an exact variational (mean field) theory, and both positive and negative temperature equilibria are permitted (with the latter sometimes leading to large-scale vortex structures). It will be seen that in the axisymmetric flow case, the variational approximation is not generally applicable.

A. Outline and summary of results

The outline of the remainder of this paper is as follows. The basic equations of motion, derived from the 3D Euler equation under the axial flow assumption and reduced to a pair of coupled 2D equations for ξ and σ (defined on the poloidal plane), are summarized in Sec. II. The key conservation laws are summarized in Sec. III. In addition to the usual kinetic energy, linear momentum along the cylinder axis, and angular momentum about the axis, these include two infinite classes of conserved circulation integrals that are a consequence of the constrained effectively 2D dynamics. The first class involves σ alone. The second couples both fields, but only linearly in ξ. All of the conserved values may be viewed as fixed by the flow initial condition, and then maintained through the turbulent cascade that leads to the late-time equilibrated flow.

In Sec. IV the thermodynamic free energy fully characterizing the equilibrium flows is defined in terms of the underlying grand canonical statistical mechanics formalism laid out in Appendices A and B. The continuum fluid results are obtained through a limiting procedure in which the continuous poloidal plane is replaced by a 2D grid with microscopic mesh size a, and the limit $a \to 0$ taken. Similar to the Euler case [3], it transpires that the temperature and other model parameters must be scaled appropriately with a to obtain a sensible thermodynamic limit. At this point the basic positive temperature requirement is an obvious consequence of the unboundedness of the poloidal field ξ, which is then capable of absorbing arbitrarily large energies.

To gain basic intuition, in Sec. V the exact solution is derived for the special choice of parameters in which the toroidal and poloidal degrees of freedom are completely decoupled. This solution will turn out to be highly relevant to the general case as well. We also introduce a class of "finite-level" models in which the full set of conserved integrals are constrained to a finite number through a special choice of parameters. These are particularly amenable to analytic and numerical solution.

In Sec. VI the full coupled model is considered, and reduced models are derived focusing separately on the toroidal and poloidal fields. In particular, by integrating out the poloidal field ξ, the effective theory for σ is shown to be equivalent to a certain type of classical antiferromagnetic (AF) spin model on the microgrid. Proper scaling in the $a \to 0$ limit, however, turns out to generate only very weak antiferromagnetic correlations, allowing an exact perturbative treatment of both classes of conservation laws. The intuition here is that the bias on ξ introduced by the second class of conservation laws is rather weak compared to the intrinsic microscale fluctuations, and the final result lies very close to the decoupled model solution.

On the other hand, the effective theory for ξ, obtained by integrating out the toroidal field σ, is that of a plasma model with long-range logarithmic (2D Coulomb-type) interactions—as would be expected from the underlying vortex degrees of freedom. The AF correlations are here reflected in the strong tendency toward local charge neutrality in Coulomb systems, which includes also the classic electrostatic effect in which all uncompensated free charges are pushed to the system boundary. There they are distributed in such a way as to produce vanishing interior large-scale flow (equivalent to the requirement of vanishing static electric field within a conducting body).

In Sec. VII some simple examples are treated, including a detailed look at the two-level model, and are used to illustrate the general theory.

The paper is concluded in Sec. VIII. In particular, comparison is made with the approach of Ref. [20] (motivated as well by earlier work [21]) in which an artificial cutoff $|\xi| < M$ is applied, and the limit $M \to \infty$ taken after $a \to 0$. These two limits do not generally commute and this strongly impacts the physical consequences of the theory. In particular, the variational approach used there, indeed valid in parameter regimes where $|\xi| = O(M)$ is controlled by the cutoff, is seen here to fail when the dynamics fully encompasses a very large range of scales—from finite $|\xi| \ll M$ all the way up to $|\xi| \sim 1/a$ controlled by microscale mixing processes—hence, missing the effects of strong positive temperature fluctuations. However, the large-scale (negative temperature) poloidal eddy structures emerging from this theory do mirror (and were motivated by) experimental results on this system (see, e.g., Refs. [23,24] and references therein), and seen as well in more recent direct numerical simulations [25,26]. Given the macroscopically featureless poloidal flows predicted here, this raises very interesting questions about violations of ergodicity and other full equilibration barriers (previously observed in Euler flows [27,28]) that deserve more careful investigation. Further refinement of the proper theoretical description of such long-lived (negative-temperature-like) states will hopefully be informed by the physics of the exact equilibrium theory presented here.

It may be observed that fluid equilibria provide a wonderful, self-consistent theoretical playground. The statistical assumptions underlying the theory mean that they do not always fully reflect reality; however, they continue to provide tremendous insight into the physics of fluid flow.

II. BACKGROUND

In this and the following section we summarize the key properties of axisymmetric flow that allow one to derive an effective two-dimensional description with an infinite hierarchy of conservation laws. These properties are well known [12,20–22,29] but are collected here for clarity and to establish notation.

Axisymmetric flows are confined to a 3D domain of revolution with cylindrical coordinates $(\theta, r, z) \in \mathcal{D} \equiv [0, 2\pi) \times D$, where D is a fixed 2D domain in the rz plane (Fig. 1). Ultimately, we will specialize to a finite cylindrical domain, $R_{\text{in}} \leqslant r \leqslant R_{\text{out}}$, with periodic boundary conditions along the axis of the cylinder $0 \leqslant z \leqslant h$, but for now D is arbitrary.

The flows obey the three-dimensional Euler equation

$$\partial_t \mathbf{v} + (\mathbf{v} \cdot \nabla)\mathbf{v} = -\nabla p, \tag{1}$$

in which the pressure is uniquely determined by the incompressibility constraint

$$\nabla \cdot \mathbf{v} = 0 \tag{2}$$

but specialized to velocity fields

$$\mathbf{v} = v_r(r,z)\hat{\mathbf{r}} + v_z(r,z)\hat{\mathbf{z}} + v_\theta(r,z)\hat{\boldsymbol{\theta}}, \tag{3}$$

whose cylindrical coordinate components are independent of the azimuthal angle θ.

A. Vorticity and stream function

It follows from Eq. (2) that

$$\partial_r(rv_r) + \partial_z(rv_z) = 0, \tag{4}$$

allowing one to represent

$$v_r = -\frac{1}{r}\partial_z\psi, \quad v_z = \frac{1}{r}\partial_r\psi \tag{5}$$

in terms of a stream function $\psi(r,z)$. The velocity is therefore conveniently represented in the form

$$\mathbf{v} = \boldsymbol{\nabla} \times \left(\frac{1}{r}\psi\hat{\theta}\right) + \frac{1}{r}\sigma\hat{\boldsymbol{\theta}}, \tag{6}$$

in which ψ and the vertical component of the angular momentum density

$$\sigma = rv_\theta \tag{7}$$

about the symmetry axis are taken as the fundamental fields.

The axial vorticity ω_θ is related to the stream function by

$$\omega_\theta \equiv \hat{\mathbf{z}} \cdot \boldsymbol{\nabla} \times \mathbf{v} = \partial_z v_r - \partial_r v_z = -\frac{1}{r}\partial_z^2\psi - \partial_r\left(\frac{1}{r}\partial_r\psi\right). \tag{8}$$

Defining the poloidal (scaled) vorticity

$$\xi = \frac{\omega_\theta}{r}, \tag{9}$$

and the modified radial and 2D coordinates

$$y = \frac{r^2}{2}, \quad \boldsymbol{\rho} = (y,z), \tag{10}$$

one may express the poloidal velocity components in the form

$$\begin{aligned}(v_r, v_z) &= \left(-\frac{1}{\sqrt{2y}}\partial_z\psi, \partial_y\psi\right) \equiv \boldsymbol{\nabla}_* \times \psi \\ \boldsymbol{\nabla}_* &\equiv \hat{\mathbf{y}}\partial_y + \hat{\mathbf{z}}\frac{1}{\sqrt{2y}}\partial_z,\end{aligned} \tag{11}$$

and one obtains the relation

$$\xi = -\left(\frac{1}{2y}\partial_z^2 + \partial_y^2\right)\psi \equiv -\Delta_*\psi. \tag{12}$$

For a simply connected domain, the free slip condition is enforced with Dirichlet boundary conditions, $\psi|_{\partial D} = 0$. The generalized Laplace equation may be solved to derive ψ from any given ξ:

$$\psi(\boldsymbol{\rho}) = \int_D d\boldsymbol{\rho}' G(\boldsymbol{\rho}, \boldsymbol{\rho}')\xi(\boldsymbol{\rho}'), \tag{13}$$

with generalized Laplacian Green function obeying

$$-\Delta_* G(\boldsymbol{\rho}, \boldsymbol{\rho}') = \delta(\boldsymbol{\rho} - \boldsymbol{\rho}'). \tag{14}$$

and satisfying the same Dirichlet boundary condition in both arguments.

More generally, for the multiply connected cylindrical geometry of primary interest here, free slip boundary conditions allow different constant values of ψ on the inner and outer boundaries of the cylinder, $r_{\rm in} \leqslant r \leqslant r_{\rm out}$ [18]. This may be handled by accounting for the mean vertical flow

$$v_z^0 = \frac{1}{V_{\mathcal{D}}} \int_{\mathcal{D}} d\mathbf{x} v_z, \tag{15}$$

in which $V_{\mathcal{D}} = \pi h(r_{\rm out}^2 - r_{\rm in}^2) = 2\pi h(y_{\rm out} - y_{\rm in})$ is the cylinder volume, with h its height. Conservation of vertical momentum implies that v_z^0 is a constant of the motion (see Sec. III C), and the subtracted stream function

$$\psi_D = \psi - v_z^0 y \tag{16}$$

may be chosen to vanish on both boundaries. The scaled vorticity remains unchanged,

$$\mathbf{v}_D = \mathbf{v} - v_z^0 \hat{\mathbf{z}} \;\Rightarrow\; \xi = -\Delta_* \psi_D, \tag{17}$$

and Eq. (13) therefore generalizes to

$$\psi(\boldsymbol{\rho}) = \psi_D(\boldsymbol{\rho}) + v_z^0 y = \int_D d\boldsymbol{\rho}' G(\boldsymbol{\rho}, \boldsymbol{\rho}') \xi(\boldsymbol{\rho}') + v_z^0 y, \tag{18}$$

in which v_z^0 is a fixed parameter defined, e.g., by the flow initial condition.

B. Equations of motion in terms of ξ and σ

The azimuthal component of the Euler equation takes the form

$$\partial_t v_\theta + v_r \partial_r v_\theta + v_z \partial_z v_\theta + \frac{v_\theta v_r}{r} = 0, \tag{19}$$

which reduces to

$$\partial_t \sigma + \mathbf{w} \cdot \boldsymbol{\nabla}_{\boldsymbol{\rho}} \sigma = 0, \tag{20}$$

in which $\boldsymbol{\nabla}_{\boldsymbol{\rho}} = (\partial_y, \partial_z)$ is a 2D gradient, and

$$\mathbf{w} = \boldsymbol{\nabla}_{\boldsymbol{\rho}} \times \psi = (-\partial_z \psi, \partial_y \psi) = (r v_r, v_z) \tag{21}$$

satisfies the 2D incompressibility condition

$$\boldsymbol{\nabla}_{\boldsymbol{\rho}} \cdot \mathbf{w} = 0. \tag{22}$$

Equation (20) expresses the fact that, in this modified 2D coordinate system, the toroidal flow parameter σ is freely advected by the incompressible poloidal flow generated by ξ.

Applying appropriate spatial derivatives to the Euler equation and using the incompressibility constraint Eq. (4), the axial vorticity Eq. (8) obeys

$$\partial_t \omega_\theta + v_r \partial_r \omega_\theta + v_z \partial_z \omega_\theta - \frac{\omega_\theta v_r}{r} = \frac{\partial_z v_\theta^2}{r}, \tag{23}$$

which may be put in the form

$$\partial_t \xi + \mathbf{w} \cdot \boldsymbol{\nabla}_{\boldsymbol{\rho}} \xi = \frac{\partial_z \sigma^2}{4y^2}. \tag{24}$$

Thus, 2D advection of ξ (by its self-generated poloidal flow field) is forced by σ.

Equations (20) and (24) are the fundamental equations of motion for axisymmetric flow, reducing the 3D vector Euler Eq. (1) to a pair of coupled 2D scalar equations. The original 3D velocity field is recovered using Eq. (7), and by constructing the 2D stream function Eq. (18), and then using Eq. (5) in conjunction with the coordinate mapping Eq. (10).

III. CONSERVATION LAWS

A. Conserved energy

The kinetic energy is

$$E = \frac{1}{2}\int_{\mathcal{D}} d\mathbf{x}|\mathbf{v}|^2 = \frac{1}{2}\int_{\mathcal{D}} d\mathbf{x}\left[|\mathbf{v}_D|^2 + \left(v_z^0\right)^2\right] = \pi\int_D d\boldsymbol{\rho}\left[|\nabla_* \psi_D|^2 + \frac{\sigma^2}{2y}\right] + E_z^0$$
$$= \pi\int d\boldsymbol{\rho}\left(\xi\psi_D + \frac{\sigma^2}{2y}\right) + E_z^0 = E_G[\xi] + \pi\int d\boldsymbol{\rho}\frac{\sigma^2}{2y} + E_z^0, \tag{25}$$

in which

$$E_z^0 = \tfrac{1}{2}V_{\mathcal{D}}\left(v_z^0\right)^2, \quad E_G[\xi] = \pi\int_D d\boldsymbol{\rho}\int_D d\boldsymbol{\rho}'\xi(\boldsymbol{\rho})G(\boldsymbol{\rho},\boldsymbol{\rho}')\xi(\boldsymbol{\rho}') \tag{26}$$

are the kinetic energies associated, respectively, with the mean and poloidal flows. To derive the latter, Eq. (18) has been used following an integration by parts. The surface term vanishes by virtue of the ability to impose $\psi_D|_{\partial D} = 0$.

Energy conservation (which does not require axisymmetry) is verified by noting that, using the Euler Eq. (1) and the incompressibility condition Eq. (2), the equation of motion for the kinetic energy density

$$\varepsilon = \tfrac{1}{2}|\mathbf{v}|^2 \tag{27}$$

takes the form of the conservation law

$$\partial_t\varepsilon + \nabla\cdot\mathbf{j}_\varepsilon = 0, \tag{28}$$

with energy current

$$\mathbf{j}_\varepsilon = (p+\varepsilon)\mathbf{v}. \tag{29}$$

It follows that

$$\partial_t E = -\int_{\mathcal{D}} d\mathbf{x}\nabla\cdot\mathbf{j}_\varepsilon = -\int_{\partial\mathcal{D}} dA(p+\varepsilon)\mathbf{v}\cdot\hat{\mathbf{n}} = 0. \tag{30}$$

The surface integral over the boundary $\partial\mathcal{D}$ vanishes for any combination of periodic and free slip boundary conditions ($\mathbf{v}\cdot\hat{\mathbf{n}} = 0$).

B. Conserved vorticity integrals

It follows from Eqs. (20) and (22) that any function $f(\sigma)$ obeys the conservation law

$$\partial_t f(\sigma) + \nabla_{\boldsymbol{\rho}}\cdot[f(\sigma)\mathbf{w}] = 0. \tag{31}$$

The vorticity integral

$$\Omega_f = \int_D d\boldsymbol{\rho} f(\sigma) \tag{32}$$

then obeys

$$\partial_t\Omega_f = -\pi\int_D d\boldsymbol{\rho}\nabla_{\boldsymbol{\rho}}\cdot[f(\sigma)\mathbf{w}] = -\int_{\partial D} dl f(\sigma)\mathbf{w}\cdot\hat{\mathbf{n}} = 0. \tag{33}$$

Here, we make use of the fact that the free slip boundary condition is equivalent to $\mathbf{w}\cdot\hat{\mathbf{n}}=0$ in the modified coordinates, and is valid for arbitrary D. The special case $f(\sigma)=\sigma$ coincides with conservation of total angular momentum about the symmetry axis.

More generally, from Eqs. (20), (22), and (24) the combination $\xi f(\sigma)$ obeys

$$\partial_t[\xi f(\sigma)]+\boldsymbol{\nabla}_{\boldsymbol{\rho}}\cdot[\xi f(\sigma)\mathbf{w}]=\frac{f(\sigma)\partial_z\sigma^2}{4y^2}, \tag{34}$$

from which follows the conservation law form

$$\partial_t[\xi f(\sigma)]+\boldsymbol{\nabla}_{\boldsymbol{\rho}}\cdot\left[\xi f(\sigma)\mathbf{w}+\frac{F(\sigma)}{4y^2}\hat{\mathbf{z}}\right]=0, \tag{35}$$

in which $F(\sigma)$ obeys

$$F'(\sigma)=2\sigma f(\sigma)\;\Rightarrow\;F(\sigma)=2\int_0^\sigma sf(s)ds. \tag{36}$$

The integral

$$\tilde{\Omega}_f=\int_D d\boldsymbol{\rho}\xi f(\sigma) \tag{37}$$

therefore obeys

$$\partial_t\tilde{\Omega}_f=-\int_{\partial D}dl\frac{F(\sigma)}{4y^2}\hat{\mathbf{z}}\cdot\hat{\mathbf{n}}, \tag{38}$$

which vanishes for a cylindrical boundary $r_{\rm in}\leqslant r\leqslant r_{\rm out}$ (enforcing $\hat{\mathbf{z}}\cdot\hat{\mathbf{n}}=0$) along with periodic boundary conditions in $0\leqslant z<h$.

The interpretation here is that in addition to being self-advected by $\mathbf{w}$, the axial vorticity ξ is advected vertically by the angular momentum density σ. Hence, only for a vertical boundary does the net advection keep ξ from effectively exiting or entering the domain.

As a special case, in the context of the axisymmetric equations, the helicity is defined as [30]

$$H=2\int_{\mathcal{D}}d\mathbf{x}v_\theta\omega_\theta=4\pi\int_D d\boldsymbol{\rho}\xi\sigma \tag{39}$$

and is conserved since it corresponds to the choice $f(s)=4\pi s$ in Eq. (37).

As illustrated in Fig. 2, the full infinite set of conserved vorticity integrals may be conveniently parameterized by the functionals

$$\gamma[\sigma](s)=\int_D d\boldsymbol{\rho}\delta[s-\sigma(\boldsymbol{\rho})],\quad\tilde{\gamma}[\xi,\sigma](s)=\int_D d\boldsymbol{\rho}\xi(\boldsymbol{\rho})\delta[s-\sigma(\boldsymbol{\rho})], \tag{40}$$

which measure, for each real value $-\infty<s<\infty$, the fractional area on which σ takes the value s, in the second case weighted by the values of ξ. Given these functions, one directly derives for any function f,

$$\Omega_f[\sigma]=\int ds\gamma[\sigma](s)f(s),\quad\tilde{\Omega}_f[\xi,\sigma]=\int ds\tilde{\gamma}[\xi,\sigma](s)f(s). \tag{41}$$

C. Conserved vertical momentum

As alluded to below Eq. (15), for the case of cylindrical boundary, translation symmetry in z implies conservation of vertical momentum

$$P_z=\int_{\mathcal{D}}d\mathbf{x}v_z=V_{\mathcal{D}}v_z^0, \tag{42}$$

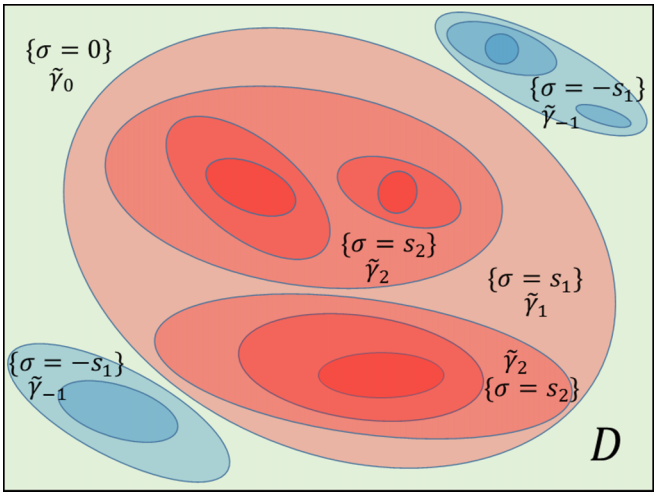

FIG. 2. Schematic level surfaces of the toroidal field σ, illustrating the conserved vorticity integrals in an approximation in which σ takes only a finite number of discrete values ($\ldots > s_2 > s_1 > 0 > -s_1 > \ldots$). As formally defined by Eq. (40), the total area $\gamma[\sigma](s)$ of each level set $\{\sigma(\boldsymbol{\rho}) = s\}$ is conserved by the flow, as is the total integral $\tilde{\gamma}[\sigma, \xi](s)$ of ξ over each such set. In general each set is the union of some number of (in general, multiply connected) pieces. For clarity, only a few of these are explicitly labeled in the figure. Since the exact value of σ, but only the mean value of ξ, is specified on each set, the former is far more strongly constrained. Arbitrary fluctuations of the latter about the mean are permitted, and this greatly impacts the predicted equilibrium states.

with or without axisymmetry. To verify this formally, the z-component of Eq. (1) may be written in the form

$$\partial_t v_z + \boldsymbol{\nabla} \cdot \mathbf{j}_z = 0, \quad \mathbf{j}_z \equiv v_z \mathbf{v} + p\hat{\mathbf{z}}, \tag{43}$$

and it follows that

$$\partial_t P_z = -\int_{\partial D} dA (v_z \mathbf{v} + p\hat{\mathbf{z}}) \cdot \hat{\mathbf{n}} = 0 \tag{44}$$

for free slip boundary conditions on a cylinder.

From Eq. (5) it follows more explicitly that

$$P_z = 2\pi h[\psi(r_{\text{out}}) - \psi(r_{\text{in}})] \tag{45}$$

is completely determined by the Dirichlet boundary conditions on ψ. In particular, as claimed earlier, $P_z = 0$ may be enforced by setting $\psi = 0$ on both boundaries.

IV. EQUILIBRIUM FREE ENERGY

The grand canonical partition function, defined by Eqs. (B1)–(B3), takes the form

$$\begin{aligned} Z &= e^{-\beta E_z^0} Z_0[\beta, \mu, \tilde{\mu}; h_\sigma, h_\xi], \\ Z_0 &\equiv \int D[\sigma] e^{-\beta \int_D d\boldsymbol{\rho} [\frac{\pi\sigma^2}{2\gamma} - \mu(\sigma) - h_\sigma(\boldsymbol{\rho})\sigma]} \int D[\xi] e^{-\beta \{E_G[\xi] - \int_D d\boldsymbol{\rho} \xi [\tilde{\mu}(\sigma) + h_\xi(\boldsymbol{\rho})]\}}, \end{aligned} \tag{46}$$

with corresponding free energy

$$F = E_z^0 + F_0[\beta, \mu, \tilde{\mu}; h_\sigma, h_\xi], \quad F_0 \equiv -\frac{1}{\beta} \ln(Z_0), \tag{47}$$

in which the functional integrals are defined by the limit Eq. (A2), and E_z^0, E_G were defined in Eq. (26). The conserved quantities are obtained from the free-energy derivatives Eq. (B5) with respect to the Lagrange multipliers $\beta, \mu, \tilde{\mu}$. We have also included conjugate fields h_σ and h_ξ that will be set to zero in the end, but whose free-energy derivatives may be used to generate statistical averages and correlations of the two fields.

We will consider first, in Sec. V, the model $\tilde{\mu} \equiv 0$, in which the two fields are entirely decoupled. This model is exact in noncylindrical geometries, where the second class of conserved integrals is absent and $\tilde{\mu}$ therefore does not appear. This limit also serves to illustrate the nature of the limit $a \to 0$. We will then consider in Sec. VI the full coupled model, in particular deriving reduced models by first integrating out either one of ξ or σ. The statistics of the remaining field exhibit rather different physical phenomena.

V. DECOUPLED MODEL

Setting $\tilde{\mu} \equiv 0$, as well as $h_\sigma = h_\xi = 0$ for now, one obtains

$$F_0(\beta, \mu) = F_\sigma(\beta, \mu) + F_\xi(\beta), \tag{48}$$

in which

$$F_\sigma = -\frac{1}{\beta} \ln(Z_\sigma), \quad F_\xi = -\frac{1}{\beta} \ln(Z_\xi), \tag{49}$$

with decoupled partition functions

$$Z_\sigma = \int D[\sigma] e^{-\beta \int_D d\boldsymbol{\rho} [\frac{\pi\sigma^2}{2y} - \mu(\sigma)]}, \quad Z_\xi = \int D[\xi] e^{-\beta E_G[\xi]}. \tag{50}$$

We analyze each in sequence, with special attention to the continuum limit, $a \to 0$. Note that when considered separately the two models may be well defined over different temperature ranges (e.g., only positive versus either sign), but in the end the sum Eq. (48) constrains the thermodynamics to a common temperature range for which both are defined (e.g., only positive).

A. Statistics of σ

Using the square grid discretization Eq. (A2) [31], the statistics of the σ field are clearly decoupled from site to site, and one obtains

$$Z_\sigma = \prod_l Z_1[\beta a^2, \mu, y_l], \tag{51}$$

with factor a^2 coming from the discretization of $\int_D d\boldsymbol{\rho}$, the product extending over all lattice sites, and single site partition function

$$Z_1(\bar{\beta}, \mu, y) = \int ds e^{-\bar{\beta}[\frac{\pi s^2}{2y} - \mu(s)]}. \tag{52}$$

Typically, the flow initial condition will have bounded σ, hence $\gamma[\sigma](s)$ has compact support, and so therefore will $e^{-\bar{\beta}\mu(s)}$. Thus, Eq. (52) is strongly convergent for any real $\bar{\beta}$, both positive and negative. The single-site probability distribution takes the form

$$p_\sigma(s, y) = \langle \delta[s - \sigma(\boldsymbol{\rho})] \rangle = \frac{e^{-\beta a^2 [\frac{\pi s^2}{2y} - \mu(s)]}}{Z_1(\beta a^2, \mu, y)}, \tag{53}$$

and the position-dependent mean is

$$\langle \sigma(\boldsymbol{\rho}) \rangle = \int s ds p_\sigma(s, y). \tag{54}$$

Equation (51) serves to illustrate another key result. It is seen that the *properly scaled thermal variable* is

$$\bar{\beta} = \beta a^2 \;\Rightarrow\; \bar{T} = T/a^2, \tag{55}$$

which needs to remain finite in the continuum limit $a \to 0$ [3]. Only for finite $\bar{\beta}$ does σ have a nontrivial distribution. The σ field free energy

$$F_\sigma(\bar{\beta}, \mu) = -\lim_{a\to 0} \frac{1}{\beta} \ln(Z_\sigma) = -\frac{1}{\bar{\beta}} \int_D d\boldsymbol{\rho} \ln[Z_1(\bar{\beta}, \mu, y)] \tag{56}$$

is also finite in the continuum limit. The latter corresponds to the thermodynamic limit in the sense that the number of grid cells $V_{\mathcal{D}}/\pi a^2$ diverges. For cylindrical $\mathcal{D}$ this expression may clearly be simplified, but in this section we treat this as a special case of the more general domain.

Finite β, in contrast, leads to $\bar{\beta} = \beta/a^2 \to \infty$ and $\bar{T} = Ta^2 \to 0$. The zero temperature limit leads to frozen $\sigma = s_0(y)$ at the value s_0 minimizing ($\beta > 0$) or maximizing ($\beta < 0$) the exponent $\frac{\pi s^2}{2y} - \mu(s)$ over the support of μ. More generally, positive temperatures encourage larger σ values to gather at smaller radii (larger $1/2y$), while negative temperatures encourage them to gather at larger radii (smaller $1/2y$) [20].

The constraint Eq. (B5) for the conserved integral $g(s)$ takes the explicit form

$$g(s) = -\frac{\delta F_\sigma}{\delta \mu(s)} = \int_D d\boldsymbol{\rho} p_\sigma(s, y). \tag{57}$$

Using independence of the two fields in the decoupled model, one obtains trivially

$$\tilde{g}(s) = \int_D d\boldsymbol{\rho} \langle \xi(\boldsymbol{\rho}) \delta[s - \sigma(\boldsymbol{\rho})] \rangle = \int_D d\boldsymbol{\rho} \langle \xi(\boldsymbol{\rho}) \rangle p_\sigma(s, y) \equiv 0, \tag{58}$$

since $E_G[\xi]$ is a positive even functional of ξ.

B. Finite-level models

A common approximation is to restrict the initial condition for σ to a finite, discrete set of levels. As the simplest model, which will form the basis for most explicit examples in later sections, the two-level system is described by

$$g(s) = A_D[p_1 \delta(s - s_1) + p_2 \delta(s - s_2)], \tag{59}$$

with, by convention, $s_2 > s_1$, and in which $A_D = \int_D d\boldsymbol{\rho} = V_{\mathcal{D}}/2\pi$ is the modified coordinate area of D, and $p_1, p_2 = 1 - p_1$ are, respectively, the fractional areas on which $\sigma(\boldsymbol{\rho}) = s_1, s_2$. The corresponding chemical potential must take the general form

$$e^{\bar{\beta}\mu(s)} = e^{\bar{\beta}\mu_1} \delta(s - s_1) + e^{\bar{\beta}\mu_2} \delta(s - s_2), \tag{60}$$

which leads to

$$\begin{aligned}
Z_1 &= e^{\bar{\beta}(\mu_1 - \pi s_1^2/2y)} + e^{\bar{\beta}(\mu_2 - \pi s_2^2/2y)}, \\
p_\sigma(s_1, y) &= 1 - p_\sigma(s_2, y) = \frac{e^{\bar{\beta}[\pi(s_2^2 - s_1^2)/4y - \mu_\Delta]}}{2\cosh\left\{\bar{\beta}\left[\pi\left(s_2^2 - s_1^2\right)/4y - \mu_\Delta\right]\right\}}, \\
\langle \sigma(\boldsymbol{\rho}) \rangle &= s_1 p_\sigma(s_1, y) + s_2 p_\sigma(s_2, y), \\
F_\sigma &= \frac{\pi\left(s_1^2 + s_2^2\right)}{4} I_D - \mu_0 A_D - \frac{1}{\bar{\beta}} \int_D d\boldsymbol{\rho} \ln\left(2\cosh\left\{\bar{\beta}\left[\frac{\pi\left(s_2^2 - s_1^2\right)}{4y} - \mu_\Delta\right]\right\}\right),
\end{aligned} \tag{61}$$

in which we define the mean and difference chemical potentials

$$\mu_0 = \frac{\mu_2 + \mu_1}{2}, \quad \mu_\Delta = \frac{\mu_2 - \mu_1}{2} \tag{62}$$

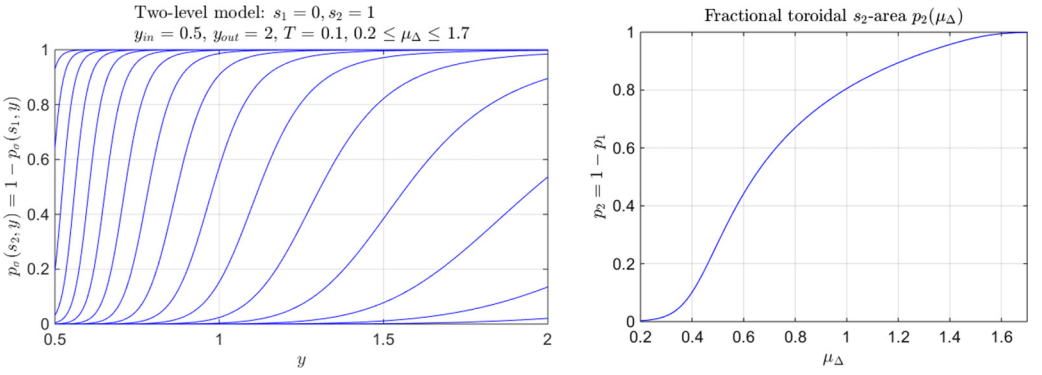

FIG. 3. Example equilibrium results for the two-level model described by Eqs. (59)–(64) using $s_1 = 0$ and $s_2 = 1$, scaled temperature $\bar{T} = 0.1$, and cylinder boundaries $r_{\text{in}} = 1$, $r_{\text{out}} = 2$ yielding $y_{\text{in}} = 0.5$, $y_{\text{out}} = 2$. Left: Probability distribution $p_\sigma(s_2, y)$ for a range of chemical potential values $0.2 \leqslant \mu_\Delta \leqslant 1.7$ in steps of 0.1. The interface moves left (larger region occupied by s_2) for increasing μ_Δ. For the chosen s_1, s_2 values, the curves coincide with the mean toroidal flow profile $\langle \sigma(\boldsymbol{\rho}) \rangle$ [third equality in Eq. (61)]. Right: Fractional area $p_2(\mu_\Delta)$, defined by Eqs. (59) and (64), occupied by $\sigma = s_2$. This illustrates the 1–1 correspondence between the Lagrange multiplier μ_Δ and the conserved integrals $g(s)$.

and the integration constant

$$I_D = \int_D \frac{d\boldsymbol{\rho}}{y}. \tag{63}$$

The constraint Eq. (57) takes the form

$$p_1 = 1 - p_2 = \frac{1}{2A_D} \int d\boldsymbol{\rho} p_\sigma(s_1, y). \tag{64}$$

These depend only on the difference μ_Δ, which is then used to set the values of $p_{1,2}$. The correspondence is easily seen to be one-to-one and invertible. Some model results are plotted in Fig. 3. For example, at low temperatures it is seen that there is sharp (Fermi-surface-like) interface between the smaller of $|s_1|, |s_2|$ $(y < y_I)$ and the larger of $|s_1|, |s_2|$ $(y > y_I)$ dominated regions, with position $y_I = \pi(s_2^2 - s_1^2)/4\mu_\Delta$ controlled by μ_Δ.

The more general L-level model, which restricts $\sigma(\boldsymbol{\rho})$ to a discrete set of values $s_1 < s_2 < \ldots < s_L$, is described by

$$g(s) = A_D \sum_{m=1}^{L} p_m \delta(s - s_m), \quad \sum_{m=1}^{L} p_m = 1, \quad e^{\bar{\beta}\mu(s)} = \sum_{m=1}^{L} e^{\bar{\beta}\mu_m} \delta(s - s_m), \tag{65}$$

which leads to

$$Z_1 = \sum_{m=1}^{L} e^{-\bar{\beta}\pi s_m^2/2y} e^{\bar{\beta}\mu_m}, \quad F_\sigma = -\frac{1}{\bar{\beta}} \int_D d\boldsymbol{\rho} \ln \left(\sum_{m=1}^{L} e^{\bar{\beta}\mu_m} e^{-\bar{\beta}\pi s_m^2/2y} \right). \tag{66}$$

Defining $m_0 = \arg\min\{|s_m|\}$ (the index of the smallest magnitude $|s_m|$), the constraint equations may be put in the form

$$p_m = \frac{1}{A_D} \int_D d\boldsymbol{\rho} p_\sigma(s_m, y), \quad p_\sigma(s_m, y) = \frac{e^{\bar{\beta}\Delta\mu_m} e^{-\bar{\beta}\pi(s_m^2 - s_{m_0}^2)/2y}}{1 + \sum_{m' \neq m_0}^{L} e^{\bar{\beta}\Delta\mu_{m'}} e^{-\bar{\beta}\pi(s_{m'}^2 - s_{m_0}^2)/2y}}, \tag{67}$$

with the differences $\Delta\mu_m = \mu_m - \mu_{m_0}$, $m \neq m_0$, used to set the $L-1$ independent p_m values. The areas $A_m = A_D p_m$ on which $\sigma = s_m$ are conserved by the flow, though the corresponding domain geometries strongly mix at ever finer scales as time advances.

Analogous to the result for the two-level model, each difference $\Delta\mu_m$ controls the position of an interface, at position $y_m = (s_m^2 - s_{m_0}^2)/2\Delta\mu_m$, separating s_m-increasingly-present ($y > y_m$) and s_m-increasingly-absent ($y < y_m$) regions.

C. Statistics of ξ

Since $E_G[\xi]$ is positive definite, Eq. (46) makes sense only for positive temperatures, $\beta > 0$. This is in contrast to the Euler equation [1,3], where the equivalent of the field ξ is directly constrained by the conservation laws, and negative temperature equilibria are ubiquitous.

To verify that the combination $\bar{\beta}$ is appropriate here as well, consider the square grid Gaussian form

$$e^{-\beta E_G[\xi]} = e^{-\frac{1}{2}\sum_{l,m} A_{lm}\xi_l\xi_m}, \tag{68}$$

with discrete variables

$$\xi_l = \xi(\boldsymbol{\rho}_l), \quad A_{lm} = \bar{\beta}a^2 G(\boldsymbol{\rho}_l, \boldsymbol{\rho}_m). \tag{69}$$

The discrete approximation to the Green function Eq. (14) takes the form

$$-\sum_n \Delta_{ln} G(\boldsymbol{\rho}_n, \boldsymbol{\rho}_m) = \delta_{lm}, \tag{70}$$

in which

$$\Delta_{lm} = a^2[\Delta_*]_{lm} = \delta_{l+\hat{\mathbf{y}},m} - 2\delta_{lm} + \delta_{l-\hat{\mathbf{y}},m} + \frac{\delta_{l+\hat{\mathbf{z}},m} - 2\delta_{lm} + \delta_{l-\hat{\mathbf{z}},m}}{2y_l} \tag{71}$$

is the discrete (nearest-neighbor finite difference) version of the generalized Laplacian. The Dirichlet boundary conditions on G lead to the vanishing of Eq. (70) when either or both l, m lie on the boundary, hence this equation only makes sense if both indices l, m correspond to interior points of D. Thus, all terms in Eq. (71) vanish if l itself is a boundary point; and if l is an interior point, then the corresponding nearest-neighbor Kronecker δ is absent if $l + \hat{\boldsymbol{\delta}}$ is a boundary point (with $\hat{\boldsymbol{\delta}}$ any of the four nearest-neighbor directions).

Put another way, from the fact that boundary values of ξ do not contribute to E_G it follows that $\sum_m G_{lm}\xi_m \equiv 0$ for any ξ entirely supported on the boundary. Thus, the matrix G is not invertible unless restricted to the interior. It follows also that, to obtain a finite well-defined free energy, the functional integral over ξ must be restricted to interior points as well. Note that since the σ field is strongly regularized, whether or not one includes values on the boundary is of negligible consequence in the continuum limit, but for consistency we will restrict it to interior sites as well.

1. Poloidal field correlations

With this interior restriction, $-\Delta_{lm}$ is precisely the inverse of the matrix G_{lm}, and the second moments of ξ are given by the corresponding nearest-neighbor form

$$\langle \xi_l \xi_m \rangle = [A^{-1}]_{lm} = -\frac{\Delta_{lm}}{\bar{\beta}a^2} = -\frac{1}{\bar{\beta}}[\Delta_*]_{lm}. \tag{72}$$

The right-hand side diverges in the continuum limit: Microscopic vorticity fluctuations are extremely large. Note that, when expressed in terms of $\beta = \bar{\beta}/a^2$, Eq. (72) may be written in the form

$$\langle \xi(\boldsymbol{\rho})\xi(\boldsymbol{\rho}')\rangle = -\frac{1}{\beta}\Delta_*\delta(\boldsymbol{\rho} - \boldsymbol{\rho}'), \tag{73}$$

which is well defined in the sense of distributions. However, for finite β this leads to a much stronger divergence of the variance $\langle \xi(\boldsymbol{\rho})^2\rangle \propto 1/\beta a^4$ that will be seen to lead to unphysical states with infinite flow energy.

By substitution of Eq. (18), it is straightforward to verify the stream function correlation identity

$$\langle \psi_D(\boldsymbol{\rho})\psi_D(\boldsymbol{\rho}')\rangle = \frac{1}{\beta}G(\boldsymbol{\rho},\boldsymbol{\rho}'). \tag{74}$$

The result is finite for finite β, but the remaining short-range singularity in G still leads to a logarithmic divergence $\langle \psi_D(\boldsymbol{\rho})^2\rangle \sim \ln(A_D/a^2)$. Similarly, the microscale mean-square difference $\langle[\psi_D(\boldsymbol{\rho}) - \psi_D(\boldsymbol{\rho}')]^2\rangle \sim \beta^{-1}\ln(|\boldsymbol{\rho}-\boldsymbol{\rho}'|/a)$ increases logarithmically with separation. Both of these results reflect the thermally rough elastic surface model that emerges when E_G is written in terms of the stream function [gradient-squared form in the first line of Eq. (25)].

It is straightforward to verify that the mean energy $\langle E_G\rangle \sim A_D/2\beta a^2$ also diverges for finite β. A consistent, finite conserved value of the hydrodynamic kinetic energy emerges only if the combination $\bar{\beta} = \beta a^2$ remains finite, consistent with the scaling (55) that emerged from the statistics of σ. With this scaling, one sees that $\langle \psi_D(\boldsymbol{\rho})\psi_D(\boldsymbol{\rho}')\rangle \to 0$: the macroscopic stream function vanishes. On the other hand, consistent with finite kinetic energy, the continuum limit correlations of the 2D velocity $\mathbf{v}_D = (v_r, v_z) = (-\partial_z\psi_D/\sqrt{2y}, \partial_y\psi_D)$ take the form

$$\langle \mathbf{v}_D(\boldsymbol{\rho})\cdot\mathbf{v}_D(\boldsymbol{\rho}')\rangle = \frac{1}{\beta}\delta(\boldsymbol{\rho}-\boldsymbol{\rho}') = \frac{1}{\bar{\beta}}\delta_{\boldsymbol{\rho},\boldsymbol{\rho}'} \tag{75}$$

and are therefore finite. Although ψ_D vanishes, and any local average of $\mathbf{v}_D$ vanishes as well, the finite microscale gradients of the former generate finite microscale velocity fluctuations containing finite energy. This is in contrast to the Euler case in which ξ is directly bounded, $\mathbf{v}_D$ is then continuous, ψ is differentiable, and the energy resides entirely in the macroscale flow. As pointed out as well in Ref. [21], there are parallels in the present case to that of magnetohydrodynamic equilibria [15], where the infinite number of integral constraints apply to the flow potentials rather than to the vorticity: finite energy again provides the essential constraint on vorticity fluctuations, and microscale velocity fluctuations make a finite contribution to the energy.

2. Poloidal field free energy

In a similar fashion, the poloidal free-energy contribution is

$$F_\xi(\bar{\beta}) = \frac{1}{2\beta}\ln[\det(\mathbf{A}/2\pi)] = -\frac{1}{2\beta}\sum_n \ln\left(\frac{2\pi a^2\lambda_n}{\bar{\beta}}\right), \tag{76}$$

in which λ_n are the eigenvalues of the generalized Poisson equation

$$-\sum_m \Delta_{lm}\psi_m = \lambda a^2\psi_l \;\to\; -\Delta_*\psi = \lambda\psi, \tag{77}$$

with the usual Dirichlet and periodic boundary conditions.

For the cylindrical geometry, translation invariance in z allows one to seek eigenfunctions of Eq. (77) in the form

$$\psi(\boldsymbol{\rho}) = e^{iqz}\psi_q(y), \quad q = \frac{2\pi m}{h}, \tag{78}$$

for integer $|m| \leqslant h/2a$. For each q one then solves the one-dimensional (1D) eigenvalue equation [32]

$$\left(-\partial_y^2 + \frac{q^2}{2y}\right)\psi_q = \lambda\psi_q, \tag{79}$$

with Dirichlet boundary conditions on the interval $[y_{\rm in}, y_{\rm out}]$. The eigenvalues $\lambda_{q,l}$ are substituted into Eq. (76) with $n = (q, l)$ now a double index.

For finite a there are $N_D = A_D/a^2$ eigenvalues, and one expects a finite limit

$$\Lambda_0 = \lim_{a\to 0} a^2 \sum_n \ln(a^2\lambda_n), \tag{80}$$

The continuum free energy, therefore, takes the form

$$F_\xi(\bar\beta) = \frac{1}{2\bar\beta}[\ln(\bar\beta/2\pi) - \Lambda_0], \tag{81}$$

and is finite for finite $\bar\beta$. Note that the Dirichlet boundary conditions on the eigenfunctions, which ensures that all $\lambda_n > 0$, automatically remove the boundary values of ξ from the functional integral, rendering the free energy well defined [as per the discussion below Eq. (71)].

To gain intuition using an analytic example, if one replaces $2y_l$ by unity in Eqs. (71), (77), and (79) [31], the Fourier representation is appropriate in both y and z, and one obtains eigenfunctions and eigenvalues

$$\begin{aligned}\psi(\boldsymbol{\rho}) &= \psi_{pq} e^{i(py+qz)}, \quad (p,q) = 2\pi\left(\frac{l}{y_{\rm out}-y_{\rm in}}, \frac{m}{h}\right),\\ \lambda(p,q) &= \frac{\sin^2(pa/2)+\sin^2(qa/2)}{a^2/4},\end{aligned} \tag{82}$$

for integers $|l| \leqslant (y_{\rm out} - y_{\rm in})/2a$, $|m| \leqslant h/2a$. This leads, as stated, to the finite limit

$$\Lambda_0 = A_D \int_{-\pi}^{\pi} \frac{ds_y}{2\pi} \int_{-\pi}^{\pi} \frac{ds_z}{2\pi} \ln[4\sin^2(s_y/2) + 4\sin^2(s_z/2)]. \tag{83}$$

Note that the scaling Eq. (77) yields the finite result $\lambda(\mathbf{q}) \to |\mathbf{q}|^2$ as $a \to 0$ for any finite $\mathbf{q}$—and will similarly yield a well-defined functional form when the $2y$ factor is restored in the eigenvalue equation. However, the free energy includes contributions from all scales, and the full microscale form of the eigenvalues enters Λ_0. As a consequence, the value of Λ_0 depends on the precise form of the discretization. However, the $\ln(\bar\beta/2\pi)$ term is universal and contains the essential temperature-dependent thermodynamic behavior, which is independent of the precise form of the continuum limit.

3. Stream function representation

Note also that one may use the eigen-decomposition to perform the phase space change of variable

$$\int D[\xi] = J_\xi \int D[\psi], \tag{84}$$

with (constant) Jacobian

$$J_\xi = \det\left[\frac{\partial\xi}{\partial\psi}\right] = \prod_n \lambda_n. \tag{85}$$

An alternative form for the partition function is therefore

$$\begin{aligned}Z_\xi &= J_\xi \int D[\psi] e^{-\beta E_G[\psi]},\\ E_G[\psi] &= -\frac{1}{2}\int d\boldsymbol{\rho}\,\psi\Delta_*\psi = \frac{1}{2}\int d\boldsymbol{\rho}|\boldsymbol{\nabla}_*\psi|^2.\end{aligned} \tag{86}$$

Using the eigen-decomposition to diagonalize $E_G[\psi]$, the free energy is

$$F_\xi(\bar\beta) = -\frac{1}{\beta}\ln(J_\xi) + \frac{1}{2\beta}\sum_n \ln(\beta\lambda_n/2\pi), \tag{87}$$

which, using Eq. (80), reproduces Eqs. (76) and (81).

D. Decoupled model thermodynamics

We have noted that F_σ is well defined for both positive and negative temperatures [assuming only bounded support of $g(s)$], while F_ξ [see Eq. (81)] is well defined only for positive temperatures. Physically, the toroidal flow energy

$$E_\sigma(\bar\beta,\mu) = \int_D d\boldsymbol{\rho}\int ds p_\sigma(s,y)\frac{\pi s^2}{2y} \tag{88}$$

is always finite, while the poloidal flow energy

$$E_\xi(\bar\beta) = \frac{\partial(\bar\beta F_\xi)}{\partial\bar\beta} = \frac{1}{2}\bar T \tag{89}$$

diverges as $\bar\beta \to 0^+$ ($\bar T \to +\infty$) and is strictly infinite for $\bar\beta < 0$. This linear in $\bar T$ result is a version of the equipartition principle for quadratic Hamiltonians, and was derived as well in Ref. [22] within the context of Gaussian fluctuations about a mean field approximation. It follows that arbitrarily large values of the total energy

$$E_0 = E_\sigma(\bar\beta,\mu) + \tfrac{1}{2}\bar T \tag{90}$$

are explored using only positive values of $\bar T$, with the toroidal energy saturating at the fully mixed value

$$E_\sigma(0,\mu) = \frac{\pi I_D}{2A_D}\int s^2 ds g(s), \tag{91}$$

in which one observes that $\lim_{\bar\beta\to 0} p_\sigma(s,y) = g(s)/A_D$ independent of y. All remaining energy is absorbed into ever increasing ξ fluctuations. Negative temperature toroidal states are never accessed by the combined system.

VI. GENERAL COUPLED MODEL

We consider now the full coupled model Eq. (46). The $\xi\tilde\mu(\sigma)$ coupling term is sufficiently simple that it is straightforward to perform the functional integral over either one of the fields to obtain a reduced model expressed entirely in terms of the other. The resulting models have more complex interactions, and an exact solution is not generally possible. However, general features may be understood, and approximate solutions may be derived in various limits. In fact, it will turn out that the proper $a \to 0$ scaling limit for the coupling requires that $\tilde\mu = \bar\mu a^2$ vanish with a, allowing an exact relation between $\tilde\mu$ and $\tilde g$ to be derived.

Both reduced models must produce the identical final free-energy Eq. (47), hence represent the same underlying physics, though expressed in different ways. The effective (conditional) equilibrium statistics of the fields σ and ξ provide interesting complementary views of the underlying fluctuations:

(1) The σ-model is a classical scalar spin model with local (nearest-neighbor) antiferromagnetic interactions but including also adjustable on-site potentials determined by the Lagrange multipliers μ, $\tilde\mu$ that allow one to enforce the conservation laws Eq. (B5) [with Eq. (40)].

(2) The ξ-model continues to be a vortex model with long-range Coulomb-type interactions, but now with an additional local potential. The potential is (linearly) unbounded from below, hence does not confine the ξ field to finite values as would be required for validity of the variational

approach—the variance of ξ is still $O(1/\bar{\beta}a^2)$. The forms of μ, $\tilde{\mu}$ that determine the exact shape of the potential again allow one to enforce the conservation laws.

A. Reduced σ-model

We consider first the case in which the (Gaussian) ξ integral is performed to obtain an effective model for σ alone. We apply the Gaussian identity

$$\prod_l \int_{-\infty}^{\infty} d\xi_l e^{\sum_l q_l \xi_l} e^{-\frac{1}{2}\sum_{l,m} A_{lm}\xi_l \xi_m} = \frac{1}{\sqrt{\det(2\pi \mathbf{A})}} e^{\frac{1}{2}\sum_{l,m}[\mathbf{A}^{-1}]_{lm} q_l q_m}, \tag{92}$$

valid for any positive definite (real symmetric) matrix $\mathbf{A}$. In addition to the parameters Eq. (69), we identify here

$$q_l = \bar{\beta}\{\tilde{\mu}[\sigma(\boldsymbol{\rho}_l)] + h_\xi(\boldsymbol{\rho}_l)\}, \tag{93}$$

in which $\boldsymbol{\rho}_l$ is again restricted to the interior of D, and the conjugate field h_ξ has also been reinstated.

Restoring continuum notation, it follows that the result of the ξ functional integral is

$$Z = \frac{e^{-\beta E_z^0}}{\sqrt{\det(2\pi\beta a^4 \boldsymbol{G})}} \int D[\sigma] e^{-\beta \mathcal{K}_1[\sigma]}, \tag{94}$$

with reduced σ-functional

$$\mathcal{K}_1[\sigma] = \int_D d\boldsymbol{\rho}\left\{\frac{\pi\sigma^2}{2y} - \mu(\sigma) - h_\sigma \sigma + \frac{1}{2}[\tilde{\mu}(\sigma) + h_\xi]\Delta_*[\tilde{\mu}(\sigma) + h_\xi]\right\}. \tag{95}$$

When interpreting the last term, the interior restriction allows one to take $\tilde{\mu}(\sigma)$ and h_ξ to vanish on the boundary. Note that the term

$$\tilde{M} \equiv -\frac{1}{2}\beta \int_D d\boldsymbol{\rho}\tilde{\mu}(\sigma)\Delta_*\tilde{\mu}(\sigma) = \frac{1}{2}\beta \int_D d\boldsymbol{\rho}\tilde{\mu}'(\sigma)^2 |\nabla_* \sigma|^2 \tag{96}$$

for $\beta > 0$ *favors* gradients in σ, corresponding to *antiferromagnetic* correlations at the grid scale. This is converse to the *ferromagnetic* negative temperature states encountered for the Euler equation [3], which favor smooth σ.

1. Scaling of $\tilde{\mu}(\sigma)$

In discrete form, one obtains

$$\beta\mathcal{K}_1[\sigma] = \bar{\beta}\sum_l \left[\frac{\pi\sigma_l^2}{2y_l} - \mu(\sigma_l) - h_{\sigma,l}\sigma_l\right] + \frac{\bar{\beta}}{2a^2}\sum_{l,m}\Delta_{lm}[\tilde{\mu}(\sigma_l) + h_{\xi,l}][\tilde{\mu}(\sigma_m) + h_{\xi,m}]. \tag{97}$$

The first line generates the individual spin weighting analyzed in Sec. V A. The second line generates antiferromagnetic nearest-neighbor interactions between spins. Note the appearance of the divergent coefficient $\beta = \bar{\beta}/a^2$, rather than $\bar{\beta}$, in the latter. We will see below that to obtain the proper scaling that produces finite values for the conserved integrals $\tilde{g}(s)$, one requires an additional scaling relation

$$\tilde{\mu}(\sigma) = a\bar{\mu}_0 + a^\gamma \bar{\mu}(\sigma), \quad h_\xi = a^\gamma \bar{h}_\xi \tag{98}$$

for some $\gamma > 0$, with $\bar{\mu}$ and $\bar{h}_\xi$ remaining finite as $a \to 0$. From Eq. (96) one sees that $\bar{\mu}_0$ contributes only at the boundary, but is required, with its potentially distinct scaling, to control the total vorticity $\int_D d\boldsymbol{\rho}\xi(\boldsymbol{\rho})$. The choice $\gamma = 1$ produces a finite antiferromagnetic coupling in Eq. (97). We will see that this leads to divergent $\tilde{g}(s)$, and a larger value $\gamma = 2$, hence asymptotically vanishing coupling, is required.

Physically, the coupling biases the equilibrium state toward differing neighboring toroidal flows σ, beyond that which would be encountered with pure random (Poisson statistics) assignment,

$\tilde{\mu} \equiv 0$. This is precisely what is required to control the specified nonzero average $\tilde{g}(s)$ of ξ over different level sets $\{\sigma = s\}$ [see Eqs. (40) and (B5)]. Since real fluids do not have a fixed microscale a, it is not clear how such correlations would actually be exhibited in an equilibrating fluid, especially as finite viscosity will lead to at some point to significant dissipation. As discussed in more detail in Sec. VIII, this would be an interesting topic for future numerical investigation.

2. *Equilibrium averages*

The equilibrium average of ξ follows in the form

$$\begin{aligned} \xi_{\rm eq}(\boldsymbol{\rho}) &\equiv \langle \xi(\boldsymbol{\rho})\rangle = -\frac{\delta F_0}{\delta h_\xi(\boldsymbol{\rho})} = -\langle \Delta_* \tilde{\mu}[\sigma(\boldsymbol{\rho})]\rangle = -\Delta_* \psi_{\rm eq}(\boldsymbol{\rho}), \\ \psi_{\rm eq}(\boldsymbol{\rho}) &\equiv \langle \tilde{\mu}[\sigma(\boldsymbol{\rho})]\rangle, \end{aligned} \tag{99}$$

in which the averages are now with respect to the reduced functional $\mathcal{K}_1[\sigma]$, and we set $h_\xi = 0$ at the end. The adopted convention $\tilde{\mu}[\sigma(\boldsymbol{\rho})] \equiv 0$ on ∂D ensures that $\psi_{\rm eq}$ obeys the required Dirichlet boundary conditions. Although $\tilde{\mu}(\sigma)$, like σ itself, will have strong microscale fluctuations, $\psi_{\rm eq}(\boldsymbol{\rho})$ will be a smooth function in the interior of D, and it follows that $\langle \xi(\boldsymbol{\rho})\rangle$ will be as well [33]. The scaling Eq. (98) actually results in $\psi_{\rm eq} \to 0$, while

$$\xi_{\rm eq}(\boldsymbol{\rho}) \to \bar{\mu}_0[\delta(y - y_{\rm in}) + \delta(y - y_{\rm out})], \tag{100}$$

corresponding to vanishing interior vorticity, but a pair of uniform finite vortex surface layers with total mean vorticity,

$$\xi_0 = \frac{1}{A_D}\int_D d\boldsymbol{\rho}\, \xi_{\rm eq}(\boldsymbol{\rho}) = \frac{2\bar{\mu}_0}{y_{\rm out} - y_{\rm in}}. \tag{101}$$

Unequal vortex layers generate a net uniform flow, and hence provide an equivalent mechanism for producing the conserved vertical flow v_z^0. Equal layers produce zero net interior flow, hence vanishing energy contribution. Physically, this is directly analogous to the usual Coulomb result that all excess charge on a conducting body resides on the surface in such a way that the interior electric field vanishes. Note that for $\gamma > 1$ the stream function fluctuations $\psi_D \sim a/\sqrt{\bar{\beta}}$ are much larger than those in $\tilde{\mu}(\sigma)$, and produce the finite microscale velocity fluctuations [34].

By way of contrast, if spread uniformly, $\xi(\boldsymbol{\rho}) \equiv \xi_0$, then the result is a linear shear flow

$$\psi_{\rm eq}(y) = \frac{1}{2}\xi_0(y - y_{\rm in})(y_{\rm out} - y), \quad v^z_{\rm eq}(y) = -\xi_0\left(y - \frac{y_{\rm in} + y_{\rm out}}{2}\right). \tag{102}$$

However, in the context of the Euler equation, this corresponds to a "zonal jet" negative temperature state, and is in the present case thermodynamically unstable to the positive temperature state Eq. (101).

The conserved integrals Eq. (B5) follow in the form

$$\begin{aligned} g(s) &= -\frac{\delta F_0}{\delta \mu(s)} = \int_D d\boldsymbol{\rho}\langle \delta[s - \sigma(\boldsymbol{\rho})]\rangle, \\ \tilde{g}(s) &= -\frac{\delta F_0}{\delta \tilde{\mu}(s)} = -\int_D d\boldsymbol{\rho}\langle \Delta_*\tilde{\mu}[\sigma(\boldsymbol{\rho})]\delta[s - \sigma(\boldsymbol{\rho})]\rangle, \end{aligned} \tag{103}$$

in which we have set $h_\xi = h_\sigma = 0$. The substitution $\xi \to -\Delta_*\tilde{\mu}(\sigma)$ is consistent with Eq. (99). However, although the mean Eq. (99) vanishes, the confinement of the integration support to a particular level set $\sigma = s$ in general biases the integrand defining $\tilde{g}(s)$ to produce a nonzero result. For example, if s is at the high end of the support of $g(s)$, then the neighboring points $\boldsymbol{\rho} \pm a\hat{\mathbf{y}}$, $\boldsymbol{\rho} \pm a\hat{\mathbf{z}}$ will likely lie on lower level sets, biasing the finite difference Laplacian $a^2\Delta_*\sigma(\boldsymbol{\rho})$ [see Eq. (71)] to finite negative values, and $a^2\Delta_*\bar{\mu}[\sigma(\boldsymbol{\rho})]$ to (also typically finite) values depending on the precise form of the function $\bar{\mu}(s)$.

It follows that finite biased values of $\Delta_*\tilde{\mu}[\sigma(\boldsymbol{\rho})] = a^{\gamma-2}(a^2\Delta_*)\bar{\mu}[\sigma(\boldsymbol{\rho})]$ require the choice

$$\gamma = 2, \tag{104}$$

as claimed above. This choice confirms, via Eq. (99), that the bias in ξ when $\boldsymbol{\rho}$ is confined to a particular level set of σ is also finite, as required by the original form Eq. (B5) with Eq. (40).

The total vorticity is

$$A_D\xi_0 = \int ds\tilde{g}(s) = 2h\bar{\mu}_0, \tag{105}$$

and is nonzero only by virtue of the surface layers.

3. *Exact relations for g(s) and $\tilde{g}$(s)*

With the choice Eq. (104), the last line of the statistical functional Eq. (97) is of relative order a^2 compared to the first, and it follows that the averages Eq. (103) may be evaluated using the first term alone, i.e., the uncoupled model—the additional antiferromagnetic bias (beyond the appearance of $\tilde{\mu}$ in the integrand of that equation) is negligible compared to that induced by the choice of s. This produces the following exact solution.

The conserved integral $g(s)$ is still given by Eq. (57), with input Eqs. (53) and (52).

Moving on to $\tilde{g}(s)$, since all sites are completely independent in the decoupled model, for $\boldsymbol{\rho} \neq \boldsymbol{\rho}'$, even for nearest-neighbor microscale grid sites, one obtains

$$\langle\bar{\mu}[\sigma(\boldsymbol{\rho}')]\delta[\sigma(\boldsymbol{\rho}) - s]\rangle_0 = \langle\bar{\mu}[\sigma(\boldsymbol{\rho}')]\rangle_0\langle\delta[\sigma(\boldsymbol{\rho}) - s]\rangle_0 = p_\sigma(s, y)\int ds'\bar{\mu}(s')p_\sigma(s', y'), \tag{106}$$

while, for $\boldsymbol{\rho} = \boldsymbol{\rho}'$,

$$\langle\bar{\mu}[\sigma(\boldsymbol{\rho})]\delta[\sigma(\boldsymbol{\rho}) - s]\rangle_0 = \bar{\mu}(s)\langle\delta[\sigma(\boldsymbol{\rho}) - s]\rangle_0 = \bar{\mu}(s)p_\sigma(s, y), \tag{107}$$

in which $\langle\cdot\rangle_0$ denotes the decoupled model average, $\tilde{\mu} \equiv 0$, and the single site probability p_σ is defined by Eq. (53). Substituting the discrete form Eq. (71), along with the scaling Eqs. (98) and (104), one obtains

$$\Delta_*\tilde{\mu}(\sigma_l) \to \bar{\mu}(\sigma_{l+\hat{\mathbf{y}}}) + \bar{\mu}(\sigma_{l-\hat{\mathbf{y}}}) + \frac{\bar{\mu}(\sigma_{l+\hat{\mathbf{z}}}) + \bar{\mu}(\sigma_{l-\hat{\mathbf{z}}})}{2y_l} - \left(2 + \frac{1}{y_l}\right)\bar{\mu}(\sigma_l), \tag{108}$$

as long as l does not neighbor a boundary point (i.e., $l \pm \hat{\mathbf{y}}$ are both not boundary points), while

$$-\Delta_*\tilde{\mu}(\sigma_l) \to \frac{\bar{\mu}_0}{a} \tag{109}$$

for l neighboring a boundary point.

Substituting Eqs. (107)–(109) into the second line of Eq. (103) and restoring continuum limit notation, one obtains

$$\tilde{g}(s) = \int_D d\boldsymbol{\rho}p_\sigma(s, y)\left(2 + \frac{1}{y}\right)\left[\int ds'\bar{\mu}(s')p_\sigma(s', y) - \bar{\mu}(s)\right] + h\bar{\mu}_0[p_\sigma(s, y_{\text{in}}) + p_\sigma(s, y_{\text{out}})], \tag{110}$$

in which, in the first term, one may safely replace $p_\sigma(s, y + a\hat{\boldsymbol{\delta}}) \to p_\sigma(s, y)$ for all $\hat{\boldsymbol{\delta}}$ at the end because ratios of small differences are no longer involved. The s-integral of the first term vanishes, while the last line produces Eq. (105).

Equation (110) [replacing Eq. (58)], along with Eq. (57), are the fundamental results of this section. Note that the relation between μ and g is independent of $\bar{\mu}$, but strongly nonlinear. However, once μ is determined, the relation between $\tilde{g}$ and $\bar{\mu}$ is linear. Some illustrative applications will be presented in Sec. VII.

B. Reduced ξ-model

Although the σ-field formulation Eq. (95) provides the most convenient representation, being directly expressed in terms of the conserved field, it is interesting to examine also the alternative reduced model obtained by integrating out σ. Since the latter appears without any coupling between different spatial points, we can express the result in terms of the 1D integral

$$e^{\bar{\beta}W(x,t;h_\sigma,h_\xi)} = \int ds e^{\bar{\beta}\{\mu(s)+x[\tilde{\mu}(s)+h_\xi]-\pi s^2/2t+h_\sigma s\}}, \tag{111}$$

which yields

$$Z = e^{-\beta E_z^0} \int D[\xi] e^{-\beta \mathcal{K}_2[\xi]}, \tag{112}$$

with reduced ξ-functional

$$\mathcal{K}_2[\xi] = E_G[\xi] - \int_D d\boldsymbol{\rho} W[\xi(\boldsymbol{\rho}), y; h_\sigma(\boldsymbol{\rho}), h_\xi(\boldsymbol{\rho})]. \tag{113}$$

The positions of the level curves of σ fluctuate with the statistical mechanical average, hence the statistics of ξ at each physical point $\boldsymbol{\rho}$ involve also an average over the possible σ-level curves passing through that point. This is precisely the content of the function W. As will be discussed below, this model must contain the identical antiferromagnetic interpretation as the σ formulation.

The result here is formally similar to that for the Euler equation [3], except for that case the range of ξ was directly bounded by the vorticity constraints. Here it is unbounded since the vorticity constraints instead apply to σ. For example, the two-level system form yields

$$W(x,t) = \frac{1}{\bar{\beta}} \ln\left[e^{\bar{\beta}(\mu_1+x\tilde{\mu}_1-\pi s_1^2/2t)} + e^{\bar{\beta}(\mu_2+x\tilde{\mu}_2)-\pi s_2^2/2t}\right], \tag{114}$$

in which $\tilde{\mu}_l = \tilde{\mu}(s_l)$, $l = 1, 2$. This result contains linearly increasing terms for $\mathrm{sgn}(x)$ such that $x\tilde{\mu}_l > 0$ [as should be more generally clear from the $\xi\tilde{\mu}(\sigma)$ dependence in Eq. (46)]. These are controlled by the positive definite quadratic form $E_G[\xi]$, but as a consequence there remain large fluctuations in equilibrium, and the Euler equation mean field result fails (which is a consequence *both* of the bounded vorticity and of the long-range property of G).

In the absence of W, as seen in detail in Sec. V, one has Fourier coefficient $\hat{\xi}(\mathbf{q}) \sim q/\sqrt{\bar{\beta}}$, strongly divergent at small scales, $q \sim \pi/a$, leading to $\langle \xi(\boldsymbol{\rho})^2 \rangle \sim 1/a^4 \to \infty$ [see Eq. (73)]. From the definition Eq. (111), one sees that

$$e^{\bar{\beta}W(x,t)} \sim \begin{cases} e^{\bar{\beta}\tilde{\mu}_{\max}x}, & x \to \infty \\ e^{\bar{\beta}\tilde{\mu}_{\min}x}, & x \to -\infty \end{cases}, \tag{115}$$

in which

$$\tilde{\mu}_{\max} = \sup \tilde{\mu}(s), \quad \tilde{\mu}_{\min} = \inf \tilde{\mu}(s) \tag{116}$$

are the maximum and minimum values of $\tilde{\mu}(s)$. It follows that $W(x,t) \to +\infty$ on at least one side for large $|x|$ (depending on the signs of $\tilde{\mu}_\pm$), thus enhancing, rather than suppressing, fluctuations of ξ. This contrasts with the Euler equation case, in which the analog of $W \to -\infty$ outside a finite range of support of ξ, directly limiting its fluctuations.

As in the decoupled model one therefore relies on the quadratic term E_G to counteract this divergence, and one expects a self-consistent shift in the mean of the form $\delta\xi \sim -\Delta_{\boldsymbol{\rho}} W(\xi, y) \sim (\tilde{\mu}_{\max} - \tilde{\mu}_{\min})/a^2$, accounting for the site-to-site near-independence. The finite shift requirement leads to the scaling $\tilde{\mu}_{\max,\min} = a^2\bar{\mu}_{\max,\min}$, recovering Eqs. (98) and (104). Note also that the combination $\bar{\beta}\tilde{\mu}\xi = \bar{\beta}\bar{\mu}\delta\xi a^2 \to 0$ for $\xi \sim 1/a$: the coupling term is a vanishing perturbation of the decoupled model, but is precisely the right size to provide the finite bias to the large $q \sim \pi/a$ Fourier components that dominate the microscale mixing.

The mean value $\tilde{g}(s)$ of ξ is *fixed* on each $\sigma = s$ level curve, set here through the Lagrange multiplier $\tilde{\mu}(s)$. However, there is only weak control of fluctuations about this mean, which remain comparable to those for the decoupled model. Thus, the equilibria will be strongly fluctuating and the variational mean field approximation will fail. The elastic membrane model Eq. (86) defined by the stream function ψ will fluctuate strongly, though remaining microscopically consistent with the mean values defined by $\tilde{\mu}(s)$ [see Eq. (99)] and constrained by the Dirichlet boundary condition on the domain D.

From Eq. (B5), the conserved integrals take the form

$$\begin{aligned} g(s) &= \left\langle \int_D d\boldsymbol{\rho} \frac{\delta W[\xi(\boldsymbol{\rho}), y]}{\delta \mu(s)} \right\rangle = \int_D d\boldsymbol{\rho} \langle \gamma[s|\xi(\boldsymbol{\rho})] \rangle, \\ \tilde{g}(s) &= \left\langle \int_D d\boldsymbol{\rho} \frac{\delta W[\xi(\boldsymbol{\rho}), y]}{\delta \tilde{\mu}(s)} \right\rangle = \int_D d\boldsymbol{\rho} \langle \xi(\boldsymbol{\rho}) \gamma[s|\xi(\boldsymbol{\rho})] \rangle, \end{aligned} \tag{117}$$

in which the averages are now with respect to the reduced functional $\mathcal{K}_2[\xi]$, and

$$\gamma[s|\xi(\boldsymbol{\rho})] = \langle \delta[s - \sigma(\boldsymbol{\rho})] \rangle_\sigma = e^{-\bar{\beta} W[\xi(\boldsymbol{\rho}), y]} e^{\bar{\beta}[\mu(s) + \xi(\boldsymbol{\rho})\tilde{\mu}(s) - \pi s^2/2y]} \tag{118}$$

is the probability distribution of $s = \sigma(\boldsymbol{\rho})$ for fixed $\xi(\boldsymbol{\rho})$ (with $\langle \cdot \rangle_\sigma$ being the average over σ at fixed ξ). For fixed s, Eqs. (115) and (116) control the behavior of γ for large $|\xi(\boldsymbol{\rho})|$.

Using the scaling Eqs. (98) and (104), it is straightforward to rederive the forms Eqs. (57) and (110) for the conserved integrals. Specifically, one may simply drop the $\tilde{\mu}$ dependence in the expression for $g(s)$—it generates vanishing corrections for $a \to 0$. Similarly, in the expression for $\tilde{g}$ the ξ dependence in the $e^{-\bar{\beta} W}$ factor in Eq. (118) may be dropped, and the average of the resulting combination $p_\sigma(s, y) \xi e^{\bar{\beta} \tilde{\mu}(s) \xi}$ reproduces the result Eq. (110).

VII. APPLICATIONS

We consider now a few examples, illustrating the results of the theory.

A. Uniform vorticity bias

Consider first the case of constant $\tilde{\mu}(s) = a\bar{\mu}_0$, in which only the uniform term is kept in Eq. (98). As will be seen, the long-range Coulomb interactions make this a rather singular limit. For short-range interactions, a finite uniform mean vorticity would be expected [see Eq. (102)], but, as we have previously seen, the long-range interactions push the extra vorticity to the boundaries [see Eq. (100)].

Since dependence on σ drops out, this represents a somewhat more general decoupled model [20], and it follows that the σ-field distribution function Eq. (53), free-energy Eq. (56), and conserved integrals Eq. (57) are unchanged.

The ξ-field partition function, defined by Eq. (92) with constant $q_l = \bar{\beta} a \bar{\mu}_0$, leads to the correction

$$F_\xi(\bar{\beta}, \bar{\mu}_0) = F_\xi(\bar{\beta}) - ah\bar{\mu}_0^2, \tag{119}$$

in which the first term is given by Eq. (81) and the second term is the result of the area integral of

$$-\tfrac{1}{2}\tilde{\mu}\Delta_*\tilde{\mu} = \tfrac{1}{2}a\bar{\mu}_0^2[\delta(y - y_{\text{in}}) + \delta(y - y_{\text{out}})] \tag{120}$$

or equivalently the area integral of $\frac{1}{2}|\nabla_*\tilde{\mu}|^2$. The correction vanishes in the continuum limit, consistent with the physical result that the equilibrium surface vortex layer, which continues to be defined by Eq. (100), generates vanishing bulk flow, hence negligible energy.

Note that such vortex layers exist also in positive temperature Euler equilibria [3]; however, the bounds on $|\xi|$ in that case constrain these layers to finite amplitude and finite width. Correspondingly, finite $\bar{T}$ suffices to generate "blurring" of these layers, with finite excitation of vorticity into

the system interior. The bound $|\xi| < M$ used in Ref. [20] as part of their limiting procedure for axisymmetric equilibria yields similar nonsingular equilibria if one scales $\bar{T} \propto M^2$ [35].

The ξ-dependent conserved integrals are given by the last term in Eq. (110):

$$\tilde{g}(s) = h\bar{\mu}_0[p_\sigma(s, y_{\rm in}) + p_\sigma(s, y_{\rm out})], \tag{121}$$

corresponding again to the entire shift in the mean of ξ residing on the boundaries. Consistently, one obtains

$$A_D\xi_0 = -\frac{\partial F_\xi}{\partial \tilde{\mu}_0} = 2h\bar{\mu}_0 = \int ds\tilde{g}(s), \tag{122}$$

with areal mean ξ_0 defined by Eq. (101). Thus, even though the free-energy correction in Eq. (119) is vanishingly small, it still generates the finite contribution to the $\tilde{\mu}$ derivative required for consistency with the conserved integrals.

B. Two-level system poloidal equilibria

We consider next the more interesting, nonsingular problem corresponding to the two-level system described in Sec. V B [see Eqs. (59)–(64)], where toroidal equilibrium quantities were also derived (Fig. 3). Here we extend the results to include poloidal equilibrium quantities. The four Lagrange multiplier parameters $\mu(s_1)$, $\mu(s_2)$ and $\tilde{\mu}(s_1)$, $\tilde{\mu}(s_2)$ reduce the general solution derived in Sec. VI A to a finite dimensional problem.

The form Eq. (59) restricting $\sigma = s_1, s_2$ leads to

$$\tilde{\mu}[\sigma(\boldsymbol{\rho})] = \tilde{\mu}_1\chi_{\{\sigma=s_1\}}(\boldsymbol{\rho}) + \tilde{\mu}_2\chi_{\{\sigma=s_2\}}(\boldsymbol{\rho}), \tag{123}$$

in which $\chi_A(\boldsymbol{\rho})$ is the indicator function on the set A. Note that the scaling Eqs. (98) and (104) still applies, but will only be imposed later.

Defining the Ising variable

$$\bar{\sigma} = \frac{2\sigma - (s_1 + s_2)}{s_2 - s_1} = \pm 1, \tag{124}$$

one may write

$$\mu(\sigma) = \mu_0 + \mu_\Delta\bar{\sigma}, \quad \tilde{\mu}(\sigma) = \tilde{\mu}_0 + \tilde{\mu}_\Delta\bar{\sigma}, \tag{125}$$

in which μ_0, μ_Δ were defined in Eq. (62), and similarly

$$\tilde{\mu}_0 = \frac{\tilde{\mu}_2 + \tilde{\mu}_1}{2}, \quad \tilde{\mu}_\Delta = \frac{\tilde{\mu}_2 - \tilde{\mu}_1}{2}. \tag{126}$$

Substituting Eqs. (124)–(126) into the discrete form Eq. (97) of the σ-functional, one obtains the nearest-neighbor antiferromagnetic Ising model form

$$\beta\mathcal{K}_1[\sigma] = \frac{\bar{\beta}}{2}\sum_{l,\hat{\boldsymbol{\delta}}} J_{l,\hat{\boldsymbol{\delta}}}\bar{\sigma}_l\bar{\sigma}_{l+\hat{\boldsymbol{\delta}}} - \bar{\beta}\sum_l h_l\bar{\sigma}_l + \bar{\beta}\mathcal{K}_0, \tag{127}$$

in which the $\hat{\boldsymbol{\delta}}$ sum in the first term runs over nearest neighbors $\pm\hat{\mathbf{y}}$, $\pm\hat{\mathbf{z}}$, and includes dropping of boundary terms as described below Eq. (71). The (antiferromagnetic) exchange, magnetic field, and additive parameters are given, respectively, by

$$J_{l,\pm\hat{\mathbf{y}}} = \frac{\tilde{\mu}_\Delta^2}{a^2}, \quad J_{l,\pm\hat{\mathbf{z}}} = \frac{\tilde{\mu}_\Delta^2}{2a^2y_l},$$

$$h_l = \frac{s_2 - s_1}{2}h_{\sigma,l} + \mu_\Delta - \frac{\pi(s_2 - s_1)}{4y_l} - \frac{\tilde{\mu}_\Delta}{a^2}\sum_m \Delta_{lm}(\tilde{\mu}_0 + h_{\xi,m}),$$

$$\mathcal{K}_0 = \sum_l \left[\frac{\pi(s_1^2 + s_2^2)}{4y_l} - \mu_0 - \frac{s_1 + s_2}{2} h_{\sigma,l} - \frac{\tilde{\mu}_\Delta^2}{a^2} \left(1 + \frac{1}{2y_l}\right) \right] + \frac{1}{2a^2} \sum_{l,m} (\tilde{\mu}_0 + h_{\xi,l}) \Delta_{lm} (\tilde{\mu}_0 + h_{\xi,m}). \tag{128}$$

As discussed in Sec. VI A the finite difference operations in Δ_{lm} annihilate the parameter $\tilde{\mu}_0$ except for boundary terms.

The Ising model Eq. (127), if taken at face value, has potentially very interesting thermodynamic behavior. For example, for finite values of the exchange parameters $J_{l,\hat{\delta}}$ it will undergo a magnetic transition as the temperature $\bar{T}$ falls below a critical value [36]. However, the physics of the fluid system lies entirely outside of this regime, with (perhaps unfortunately) the scaling Eqs. (98) and (104) implying asymptotically vanishing exchange parameters, but still just large enough to enforce finite values of the poloidal conserved integrals.

Example equilibrium results for the toroidal field σ were shown in Fig. 3, using $s_1 = 0$, $s_2 = 1$. We now extend these results to characterize equilibria including the poloidal field ξ. When the scaling Eq. (98) is applied, all parameters vanish except $h_l = \mu_\Delta - \pi/4y_l$, agreeing with the exponential argument in the distributions $p_\sigma(s, y)$—see Eq. (61).

The conserved integrals $\tilde{g}(s)$ may be written in the form

$$\tilde{g}(s) = A_D[p_1 \tilde{\xi}_1 \delta(s - s_1) + p_2 \tilde{\xi}_2 \delta(s - s_2)], \tag{129}$$

in which p_m are the fractional areas Eq. (64) on which $\sigma = s_m$ (and plotted in the right panel of Fig. 3), and $\tilde{\xi}_m$ are then the mean values of ξ restricted to the respective areas. From the general result Eq. (110), the latter take the form

$$\tilde{\xi}_m = \frac{1}{p_m A_D} \int_D d\boldsymbol{\rho} \tilde{G}_m(y), \tag{130}$$

with integrands

$$\tilde{G}_m(y) = p_\sigma(s_m, y) \left(2 + \frac{1}{y}\right) [\bar{\mu}_1 p_\sigma(s_1, y) + \bar{\mu}_2 p_\sigma(s_2, y) - \bar{\mu}_m] = (-1)^{m-1} 2\bar{\mu}_\Delta \tilde{G}_0(y),$$
$$\tilde{G}_0(y) \equiv \left(2 + \frac{1}{y}\right) p_\sigma(s_2, y)[1 - p_\sigma(s_2, y)]. \tag{131}$$

For simplicity, we have dropped the boundary term, setting $\bar{\mu}_0 = 0$. The integrands are equal and opposite, $\tilde{G}_1 = -\tilde{G}_2$ as required by the interior neutrality condition Eq. (100), and only the difference chemical potential $\bar{\mu}_\Delta = (\bar{\mu}_2 - \bar{\mu}_1)/2$ enters.

The function $G_0(y)$ characterizes the spatial distribution of ξ-field mean values on the two toroidal (microscopically mixed) level sets $\{\sigma = s_m\}$ whose local density is given by $p_\sigma(s_m, y)$. In fact, one may identify

$$\tilde{\xi}_m(y) = \frac{\tilde{G}_m(y)}{p_\sigma(s_m, y)} = (-1)^{m-1} 2\bar{\mu}_\Delta \left(2 + \frac{1}{y}\right) [1 - p_\sigma(s_m, y)] \tag{132}$$

as the local mean value of ξ on the respective level set at radial position y.

Figure 4 shows results for $\tilde{G}_0(y)$ and for the normalized area integral

$$\tilde{g}_0(\mu_\Delta) = \frac{1}{A_D} \int_D d\boldsymbol{\rho} \tilde{G}_0(y) \Rightarrow \tilde{\xi}_m(\mu_\Delta) = (-1)^{m-1} 2\bar{\mu}_\Delta \frac{\tilde{g}_0(\mu_\Delta)}{p_m(\mu_\Delta)}, \tag{133}$$

for the same set of μ_Δ values used in Fig. 3. The neutrality constraint $p_1 \tilde{\xi}_1 = -p_2 \tilde{\xi}_2$ implies that mean values ξ_m must increase (decrease) as their supporting area decreases (increases). Both are linear in $\tilde{\mu}_\Delta$, and the one-to-one correspondence between Lagrange multiplier and conserved integral values is therefore trivial.

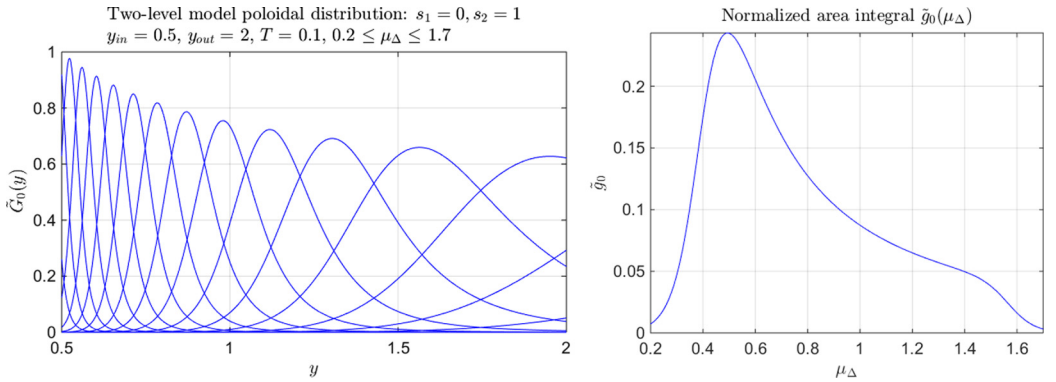

FIG. 4. Example poloidal field equilibrium results for the same two-level model and parameters described in Fig. 3. Left: Poloidal spatial distribution $\tilde{G}_0(y)$ defined by Eq. (131) for a range of chemical potential values $0.2 \leqslant \mu_\Delta \leqslant 1.7$ in steps of 0.1. The peak moves to left for increasing μ_Δ. Right: Normalized area integral $\tilde{g}_0(\mu_\Delta)$ defined by Eq. (133).

VIII. CONCLUDING REMARKS

We end by comparing the present results with the quite different axisymmetric equilibrium state predictions derived in Ref. [20] and suggest future work that might lend further insight into possible different domains of validity, depending on detailed equilibration dynamics and timescales.

A. Positive temperature states

In the approach taken in Ref. [20], in addition to the microscale a, a bound $|\xi| < M$ is applied, and the limit $M \to \infty$ is taken *after* the limit $a \to 0$ [21]. If one limits consideration, as in the present work, to finite, positive temperatures $\bar{T} > 0$, no *a priori* bound on ξ is required, and the two limits commute. This is the domain of the full fluctuation-dominated model analyzed here (see Sec. VI). We have seen that this model provides a detailed methodology for computing candidate equilibrium states for any given values of the conserved integrals.

On the other hand, the theory proposed in Ref. [20] to describe the finite $\bar{T} > 0$ "low-energy" regime is based on a variational mean field approach that, unlike the exact Gaussian analysis in Sec. V C, fails to account for strong fluctuations, and therefore can provide an at best approximate description. The result of that analysis is a return to the decoupled model described in Sec. V, with $\langle \xi \rangle$ trivially slaved to $\langle \sigma \rangle$. The decoupled model plays a central role in the present (exact) analysis as well, but in a very different way that leads to vanishing $\langle \xi \rangle$ and highlights instead the statistics of the large microscale fluctuations (Sec. VI, especially Sec. VI A 3).

B. Possibility of negative-temperature-like intermediate states

We have observed that the unbounded (Gaussian) poloidal energy $E_G[\xi]$ in Eq. (25) forbids negative temperature states, $\bar{T} < 0$—just as in standard many particle systems with unbounded kinetic energy $\sim p^2/2m$. As a consequence, high-energy initial states with, e.g., smooth large-scale (negative-temperature-like) poloidal eddies, are predicted to undergo a turbulent forward energy cascade transferring much of the energy to microscale fluctuations. Specifically, the axisymmetric equations of motion Eqs. (20) and (24) in principle provide a pathway for leakage of the flow energy into small-scale (but large amplitude $\sim 1/a$) poloidal fluctuations. The analogous feature arises in the shallow water equations [18,37], where negative temperature states are similarly ruled out and large-scale eddy energy is expected to be transferred into small-scale surface height fluctuations (with equilibria similarly sensitive to the details of the microscale lattice geometry).

However, it is well known that such energy transfers between substantially different scales can be extremely slow, if not forbidden entirely, by the fundamental constraints of 2D flow. For example, it has long been observed, in the context of the Euler equation, that there can be strong barriers to full equilibration, with, e.g., very long-lived steady [27] or even fluctuating [28] states preempting the statistical mechanics prediction, and depending strongly on initial condition. Similarly, experimental results on the axisymmetric system [23,24], as well as recent numerical simulation results [25,26], display long-lived, large-scale eddy features that have been interpreted in terms of equilibrium concepts. One may motivate such a comparison by the observation that smooth, large-scale flow states, such as those described by the variational approximation, are insensitive to the microscale, and it may take time to build up the required forward cascade.

Maintaining the $|\xi| < M$ bound provides one possible route to exploring such intermediate states within the statistical equilibrium formalism [20,21]. Fixed finite M provides an upper bound on $E_G[\xi]$, and permits negative temperature states—the "high-energy" regime considered in Ref. [20]. The imposed bounded fluctuations might be thought of now as being frozen in and swept along by the large-scale flow [21] (with similar ideas potentially applicable to the shallow water system [16]). For $\bar{T} < 0$ enhancement of fine-scale mixing is replaced by enhancement of smooth flows [see Eq. (96)]. This encourages both the σ and ξ fields to organize into high-energy, macroscopic patterns (in the Coulomb analogy, like charges attract rather than repel). In particular the resulting equilibria display large-scale poloidal flow structure, including the dipolar flows and 2D vortical eddies familiar from the Euler problem.

A consistent $M \to \infty$ limit for the mean flow may be obtained by scaling the temperature and other model parameters with M, in particular $\bar{T}^{(M)} = M^2 T^* \to \infty$ [20]. It follows that the energy and mean vorticity $\langle \xi(\boldsymbol{\rho}) \rangle$ remain finite even as $\langle \xi^2 \rangle \propto M^2 \to \infty$. The divergent temperature, however, ensures that the toroidal flow field σ is completely mixed with uniform $\langle \sigma(\boldsymbol{\rho}) \rangle$. Just as in the Euler case, the variational approach provides a formally exact description in this regime, and a mean field formalism may be developed in terms of the scaled variables to solve for $\langle \xi(\boldsymbol{\rho}) \rangle$. For any finite T^* the system is dominated by divergent fluctuations $|\xi| = O(M)$, but since we are now working in the limit $M \ll 1/a$ it is clear that the two limits do not commute in the negative temperature regime.

It would be extremely interesting to explore in more detail such practical equilibration questions for the axisymmetric model (as well as for the shallow water system), where buildup of microscale mixing (or surface height fluctuations), emergence of macroscale (negative temperature) coherent poloidal jet or vortex structures [20,23–26], or perhaps other features, may similarly occur on different (perhaps even infinite [27,28]) timescales and depending on the initial state. A real fluid with finite initial ξ field is unlikely to evolve toward a state accurately reproducing the large M states studied in Ref. [20], even if one allows M to, e.g., diverge steadily with time. However, this does not preclude derivation of similar interesting flow structures (that indeed properly reflect aspects of the observed fluid physics) from a refined theory that more rigorously reflects intermediate state dynamics. In support of the latter, the physics of the exact equilibrium theory may point to more focused numerical signatures sensitive to the transfer rate of energy into large microscale fluctuations of ξ, allowing one to identify potential bottlenecks and barriers, and more carefully quantify associated timescales. The theory motivates as well careful attention to maintenance of numerical precision in the presence of extremely large microscale fluctuations.

APPENDIX A: LIOUVILLE THEOREM

Proof of the Liouville theorem for the axisymmetric system closely follows that for the Euler equation [3]. A point in the infinite dimensional phase space Γ is defined by an instantiation of the fields $\{\xi(\boldsymbol{\rho}), \sigma(\boldsymbol{\rho})\}_{\boldsymbol{\rho}\in D}$. The phase space gradient of a functional $\mathcal{F}[\xi, \sigma]$ is defined by the infinite dimensional vector of functional derivative values

$$\nabla_\Gamma \mathcal{F} = \left[\frac{\delta \mathcal{F}}{\delta \xi(\boldsymbol{\rho})}, \frac{\delta \mathcal{F}}{\delta \sigma(\boldsymbol{\rho})} \right]_{\boldsymbol{\rho}\in D}, \tag{A1}$$

and the phase space integral

$$\int_\Gamma d\Gamma = \lim_{a\to 0} \frac{1}{\mathcal{N}(a)} \prod_i \int d\xi(\boldsymbol{\rho}_i) \int d\sigma(\boldsymbol{\rho}_i) \tag{A2}$$

is defined by independent integration over each value of the fields at each point in D. Formally, it is defined here by a procedure in which the fields are first restricted to a (finite) uniform square mesh with side a, then the limit $a \to 0$ is taken with a suitable normalization $\mathcal{N}(a)$ [31]. A probability measure $\hat{\rho}[\xi, \sigma]$ is a functional with unit phase space integral, and averages are defined by

$$\langle \mathcal{F} \rangle = \int d\Gamma \hat{\rho}[\xi, \sigma] \mathcal{F}[\xi, \sigma]. \tag{A3}$$

The equations of motion are written formally in functional form $\partial_t \xi(\boldsymbol{\rho}) = \dot{\sigma}[\xi, \sigma](\boldsymbol{\rho})$, $\partial_t \sigma(\boldsymbol{\rho}) \equiv \dot{\sigma}[\xi, \sigma](\boldsymbol{\rho})$, and the phase space vector

$$\mathbf{W}[\xi, \sigma] = [\dot{\xi}(\boldsymbol{\rho}), \dot{\sigma}(\boldsymbol{\rho})]_{\boldsymbol{\rho}\in D} \tag{A4}$$

defines a flow velocity field in phase space. The flow divergence is defined by

$$\boldsymbol{\nabla}_\Gamma \cdot \mathbf{W} \equiv \int_D d\boldsymbol{\rho} \left[\frac{\delta \dot{\xi}(\boldsymbol{\rho})}{\delta \xi(\boldsymbol{\rho})} + \frac{\delta \dot{\sigma}(\boldsymbol{\rho})}{\delta \sigma(\boldsymbol{\rho})} \right], \tag{A5}$$

and its vanishing defines an *incompressible* phase space flow. Systems with the latter property are said to obey the Liouville theorem.

A probability measure, whose time dependence $\hat{\rho}[\xi, \sigma](t) = \hat{\rho}[\xi(t), \sigma(t)]$ is defined by the evolution of the field arguments obeys the equation of motion

$$\partial_t \hat{\rho} + \boldsymbol{\nabla}_\Gamma \cdot (\hat{\rho} \mathbf{W}) = 0, \tag{A6}$$

so that the product $\hat{\rho}[\xi, \sigma](t) d\Gamma(t)$ is conserved, in which the (Lagrangian) volume element $d\Gamma(t)$ is here defined to move with the flow. An equilibrium measure $\hat{\rho}_{\rm eq}$ is by definition constant in time, and therefore obeys

$$\boldsymbol{\nabla}_\Gamma \cdot (\hat{\rho}_{\rm eq} \mathbf{W}) = 0. \tag{A7}$$

If phase space flows are incompressible, $\boldsymbol{\nabla}_\Gamma \cdot \mathbf{W} = 0$, then one obtains the constraint

$$0 = \mathbf{W} \cdot \boldsymbol{\nabla}_\Gamma \hat{\rho}_{\rm eq} = \int_D d\boldsymbol{\rho} \left[\frac{\delta \hat{\rho}_{\rm eq}}{\delta \xi(\boldsymbol{\rho})} \dot{\xi}(\boldsymbol{\rho}) + \frac{\delta \hat{\rho}_{\rm eq}}{\delta \sigma(\boldsymbol{\rho})} \dot{\sigma}(\boldsymbol{\rho}) \right] = \dot{\hat{\rho}}_{\rm eq}, \tag{A8}$$

which then states that $\hat{\rho}_{\rm eq}$ is a conserved integral. It follows that

$$\hat{\rho}_{\rm eq} = f_{\rm eq}(E[\xi, \sigma], \gamma[\sigma](\cdot), \tilde{\gamma}[\xi, \sigma](\cdot)) \tag{A9}$$

must be some (ordinary) function of the basic set of conserved quantities, in the present case those defined in Sec. III. The choice of $f_{\rm eq}$ defines the statistical ensemble—see Appendix B.

We now proceed to verify phase space incompressibility (Liouville's theorem) using the equations of motion Eqs. (20) and (24). Since, via Eqs. (13) and (21), the velocity field $\mathbf{w}$ depends only on ξ, one obtains

$$\frac{\delta \dot{\sigma}(\boldsymbol{\rho})}{\delta \sigma(\boldsymbol{\rho})} = -\mathbf{w}(\boldsymbol{\rho}) \cdot \boldsymbol{\nabla}_{\boldsymbol{\rho}} \delta(\mathbf{0}) = 0. \tag{A10}$$

Here one formally concludes that $\boldsymbol{\nabla}_{\boldsymbol{\rho}} \delta(\mathbf{0}) = 0$ because $\delta(\boldsymbol{\rho})$ is formally an even function. An alternative limiting procedure would note that the symmetric finite difference $[\xi(\boldsymbol{\rho} + \mathbf{a}/2) - \xi(\boldsymbol{\rho} - \mathbf{a}/2)]/a$, for arbitrary small displacement $\mathbf{a}$, is independent of $\xi(\boldsymbol{\rho})$, hence leads to vanishing functional derivative for arbitrarily small grid cutoff $a \to 0$.

Similarly, one obtains

$$\frac{\delta\dot{\xi}(\boldsymbol{\rho})}{\delta\xi(\boldsymbol{\rho})} = -\mathbf{w}(\boldsymbol{\rho})\cdot\boldsymbol{\nabla}_{\boldsymbol{\rho}}\delta(\mathbf{0}) - \mathbf{w}_0(\boldsymbol{\rho})\cdot\boldsymbol{\nabla}_{\boldsymbol{\rho}}\xi(\boldsymbol{\rho}), \tag{A11}$$

in which $\mathbf{w}_0(\boldsymbol{\rho})$ is the self-induced advection velocity for a point vortex at $\boldsymbol{\rho}$:

$$\mathbf{w}_0(\boldsymbol{\rho}) = [\boldsymbol{\nabla}_{\boldsymbol{\rho}} \times G(\boldsymbol{\rho}, \boldsymbol{\rho}')]_{\boldsymbol{\rho}'=\boldsymbol{\rho}}. \tag{A12}$$

Although the Green function G, obeying Eq. (14) with generalized Laplacian operator defined by Eq. (12), has a logarithmic singularity at $\boldsymbol{\rho}' = \boldsymbol{\rho}$, one may still derive a sensible form for $\mathbf{w}_0$. To see this, one separates

$$G(\boldsymbol{\rho}, \boldsymbol{\rho}') = G_F(\boldsymbol{\rho}, \boldsymbol{\rho}') + \Phi(\boldsymbol{\rho}, \boldsymbol{\rho}') \tag{A13}$$

into free and boundary-induced parts, both symmetric in their arguments, and with Φ satisfying the generalized Laplace equation

$$\Delta_*\Phi = 0, \tag{A14}$$

and chosen so that G satisfies the same boundary conditions (in both arguments) discussed in Sec. II A.

In the absence of a boundary, the vortex (in this case a circular vortex ring, with unit circulation, centered on the z axis) self-advects vertically at constant speed [38,39]

$$v_F^z(y) = \frac{1}{4\pi r}\left[\ln\left(\frac{8r}{a}\right) - \frac{1}{2}\right], \quad r = \sqrt{2y}, \tag{A15}$$

which again requires a ring core radius cutoff a to properly interpret, while Φ induces an additional (regular) contribution

$$\mathbf{w}_\Phi(\boldsymbol{\rho}) = [\boldsymbol{\nabla}_{\boldsymbol{\rho}} \times \Phi(\boldsymbol{\rho}, \boldsymbol{\rho}')]_{\boldsymbol{\rho}'=\boldsymbol{\rho}} = \tfrac{1}{2}[(\boldsymbol{\nabla}_{\boldsymbol{\rho}} + \boldsymbol{\nabla}'_{\boldsymbol{\rho}}) \times \Phi(\boldsymbol{\rho}, \boldsymbol{\rho}')]_{\boldsymbol{\rho}'=\boldsymbol{\rho}} = \tfrac{1}{2}\boldsymbol{\nabla}_{\boldsymbol{\rho}} \times \Phi(\boldsymbol{\rho}, \boldsymbol{\rho}), \tag{A16}$$

in which symmetry of Φ has been used to obtain the final equality.

Finally, integrating yields

$$\begin{aligned}\int_D d\boldsymbol{\rho}\frac{\delta\dot{\xi}(\boldsymbol{\rho})}{\delta\xi(\boldsymbol{\rho})} &= -\int_D d\boldsymbol{\rho}[v_F^z(y)\hat{\mathbf{z}} + \mathbf{w}_\Phi(\boldsymbol{\rho})]\cdot\boldsymbol{\nabla}_{\boldsymbol{\rho}}\xi(\boldsymbol{\rho}) \\ &= \int_D d\boldsymbol{\rho}\xi(\boldsymbol{\rho})[\partial_z v_F^z(y) + \boldsymbol{\nabla}_{\boldsymbol{\rho}}\cdot\mathbf{w}_\Phi(\boldsymbol{\rho})] - \int_{\partial D} dA\xi(\boldsymbol{\rho})[v_F^z(y)\hat{\mathbf{z}} + \mathbf{w}_\Phi(\boldsymbol{\rho})]\cdot\hat{\mathbf{n}} \\ &= 0,\end{aligned} \tag{A17}$$

in which incompressibility of $\mathbf{w}_\Phi(\boldsymbol{\rho})$ follows directly from the final equality in Eq. (A16). The boundary term vanishes by virtue of the boundary conditions on G, which then leads to the required combination of free slip and periodic boundary conditions (described in Sec. III) on the total velocity $\mathbf{w}_0 = \mathbf{w}_\Phi + \hat{\mathbf{z}}v_F^z$.

Together, Eqs. (A10) and (A17) establish Liouville's theorem for the axisymmetric flow system.

APPENDIX B: STATISTICAL MECHANICS FORMALISM

Steady state equilibrium flows are computed using phase space averages Eq. (A3) of the flow field [1,2], with valid forms Eq. (A9) of the phase space equilibrium measure limited by the Liouville theorem.

The grand canonical equilibrium measure takes the exponential form [3]

$$\hat{\rho}_G[\xi, \sigma] = \frac{1}{Z}e^{-\beta\mathcal{K}[\xi,\sigma]}, \tag{B1}$$

in which $\beta = 1/T$ is an inverse temperature variable, and the functional $\mathcal{K}$ takes the form

$$\mathcal{K}[\xi, \sigma] = E[\xi, \sigma] - \int_D d\boldsymbol{\rho}\{\mu[\sigma(\boldsymbol{\rho})] + \xi(\boldsymbol{\rho})\tilde{\mu}[\sigma(\boldsymbol{\rho})]\}, \tag{B2}$$

being a linear sum of all of the conserved integrals, with coefficients, or Lagrange multipliers $\{\beta, \mu(\cdot), \tilde{\mu}(\cdot)\}$, defining the conjugate fields. In this case there are a pair of conjugate field *functions* $\mu(s)$, $\tilde{\mu}(s)$ (of a single argument). The mean flow/conserved momentum parameter v_z^0 is suppressed here from the notation, being assumed fixed from the outset. Its only role is to introduce the constant term [first equality in Eq. (26)].

The partition function

$$Z = \int d\Gamma e^{-\beta\mathcal{K}}, \tag{B3}$$

which simply normalizes $\hat{\rho}_G$, is related as usual to the thermodynamic free energy F via

$$F[\beta, \mu(\cdot), \tilde{\mu}(\cdot)] = -\frac{1}{\beta}\ln\{Z[\beta, \mu(\cdot), \tilde{\mu}(\cdot)]\}, \tag{B4}$$

in which a suitable $a \to 0$ continuum limiting procedure (equivalent to the thermodynamic limit in conventional systems) is implied (see Sec. IV). The equilibrium averages (with respect to $\hat{\rho}_G$) are obtained from the free-energy derivatives

$$g(s) \equiv \langle\gamma[\sigma](s)\rangle = -\frac{1}{\beta}\frac{\delta F}{\delta\mu(s)}, \quad \tilde{g}(s) \equiv \langle\tilde{\gamma}[\xi, \sigma](s)\rangle = -\frac{1}{\beta}\frac{\delta F}{\delta\tilde{\mu}(s)}, \tag{B5}$$

in which the conserved integrals γ, $\tilde{\gamma}$ are defined by Eq. (40).

By way of comparison, the microcanonical ensemble is defined by the form

$$\hat{\rho}_\mu[\xi, \sigma] = \frac{1}{W}\delta(\varepsilon - E[\xi, \sigma])\prod_s \delta(g(s) - \gamma[\sigma](s))\delta(\tilde{g}(s) - \tilde{\gamma}[\xi, \sigma](s)), \tag{B6}$$

in which each conserved integral is rigidly specified. The normalization W, which is the area of the corresponding constrained hypersurface in Γ, is related to the thermodynamic entropy via

$$S[\varepsilon, g(\cdot), \tilde{g}(\cdot)] = \ln\{W[\varepsilon, g(\cdot), \tilde{g}(\cdot)]\}. \tag{B7}$$

It is apparent that the two ensembles are related through the Laplace transform

$$\hat{\rho}_G[\xi, \sigma] = \int d\varepsilon \int D[g] \int D[\tilde{g}]\hat{\rho}_\mu[\xi, \sigma; \varepsilon, g(\cdot), \tilde{g}(\cdot)]e^{-\beta\{\varepsilon - \int ds[\mu(s)g(s) + \tilde{\mu}(s)\tilde{g}(s)]\}}, \tag{B8}$$

in which, similar to Eq. (A2), the functional integrals over g and $\tilde{g}$ may be defined via a limiting procedure,

$$\int D[g] \int D[\tilde{g}] = \lim_{\delta s \to 0} \frac{1}{\mathcal{M}(\delta s)} \prod_l \int dg(s_l) \int d\tilde{g}(s_l), \tag{B9}$$

where $\mathcal{M}$ is a normalization, and $s_l = l\delta s$, $l \in \mathbb{Z}$, represents a uniform gridding of the variable s.

Ensemble equivalence therefore reduces to the mathematical question of invertibility of this infinite dimensional Laplace transform. It is known that this property can fail in certain regions of the phase diagram [19,40], where stable free-energy minima become locally unstable saddle points. Therefore one is in general unable to access all values of the microcanonical variables through control of the conjugate field variables. However, mathematical convenience encourages one to begin with the grand canonical approach [3], which allows a more transparent exploration of the basic physics of the model, and then to subsequently investigate potential methods (e.g., some form of analytic continuation) to extend access to these technically forbidden regions.

[1] J. Miller, Statistical Mechanics of Euler Equations in Two Dimensions, Phys. Rev. Lett. **65**, 2137 (1990).
[2] R. Robert and J. Sommeria, Statistical equilibrium states for two-dimensional flows, J. Fluid Mech. **229**, 291 (1991).
[3] J. Miller, P. B. Weichman, and M. C. Cross, Statistical mechanics, Euler's equation, and Jupiter's Red Spot, Phys. Rev. A **45**, 2328 (1992).
[4] Notably, a mathematically equivalent theory of galaxy dynamics (based on the Boltzmann equation) was derived much earlier: D. Lynden-Bell, Statistical mechanics of violent relaxation in stellar systems, Mon. Not. R. Astron. Soc. **136**, 101 (1967). However, these results failed to transition to the fluid dynamics community until much later [3, 41, 42].
[5] L. Onsager, Statistical hydrodynamics, Nuovo Cimento Suppl. **6**, 279 (1949).
[6] R. H. Kraichnan, Statistical dynamics of two-dimensional flow, J. Fluid Mech. **67**, 155 (1975).
[7] D. Montgomery and G. Joyce, Statistical mechanics of "negative temperature" states, Phys. Fluids **17**, 1139 (1974).
[8] T. S. Lundgren and Y. B. Pointin, Statistical mechanics of two-dimensional vortices, J. Stat. Phys. **17**, 323 (1977); Non-Gaussian probability distributions for a vortex fluid, Phys. Fluids **20**, 356 (1977).
[9] J. Michel and R. Robert, Statistical mechanical theory of the Great Red Spot of Jupiter, J. Stat. Phys. **77**, 645 (1994).
[10] F. Bouchet and J. Sommeria, Emergence of intense jets and Jupiter's Great Red Spot as maximum-entropy structures, J. Fluid Mech. **464**, 165 (2002).
[11] P. B. Weichman, Equilibrium theory of coherent vortex and zonal jet formation in a system of nonlinear Rossby waves, Phys. Rev. E **73**, 036313 (2006).
[12] D. D. Holm, J. E. Marsden, T. Ratiu, and A. Weinstein, Nonlinear stability of fluid and plasma equilibria, Phys. Rep. **123**, 1 (1985).
[13] R. Jordan and B. Turkington, Ideal magnetofluid turbulence in two dimensions, J. Stat. Phys. **87**, 661 (1997).
[14] N. Leprovost, B. Dubrulle, and P.-H. Chavanis, Thermodynamics of MHD flows with axial symmetry, Phys. Rev. E **71**, 036311 (2005).
[15] P. B. Weichman, Long-Range Correlations and Coherent Structures in Magnetohydrodynamic Equilibria, Phys. Rev. Lett. **109**, 235002 (2012).
[16] P. B. Weichman and D. M. Petrich, Statistical Equilibrium Solutions of the Shallow Water Equations, Phys. Rev. Lett. **86**, 1761 (2001).
[17] P.-H. Chavanis and J. Sommeria, Statistical mechanics of the shallow water system, Phys. Rev. E **65**, 026302 (2002).
[18] P. B. Weichman, Competing turbulent cascades and eddy-wave interactions in shallow water equilibria, Phys. Rev. Fluids **2**, 034701 (2017).
[19] For a recent review, see F. Bouchet and A. Venaille, Statistical mechanics of two-dimensional and geophysical flows, Phys. Rep. **515**, 227 (2012).
[20] S. Thalabard, B. Dubrulle, and F. Bouchet, Statistical mechanics of the 3D axisymmetric Euler equations in a Taylor–Couette geometry, J. Stat. Mech. (2014) P01005.
[21] N. Leprovost, B. Dubrulle, and P.-H. Chavanis, Dynamics and thermodynamics of axisymmetric flows: Theory, Phys. Rev. E **73**, 046308 (2006).
[22] A. Naso, R. Monchaux, P.-H. Chavanis, and B. Dubrulle, Statistical mechanics of Beltrami flows in axisymmetric geometry: Theory reexamined, Phys. Rev. E **81**, 066318 (2010).
[23] R. Monchaux, P.-H. Chavanis, A. Chiffaudel, P. P. Cortet, F. Daviaud, P. Diribarne, and B. Dubrulle, Fluctuation-Dissipation Relations and Statistical Temperatures in a Turbulent von Kármán Flow, Phys. Rev. Lett. **101**, 174502 (2008).
[24] A. Naso, S. Thalabard, G. Collette, P.-H. Chavanis, and B. Dubrulle, Statistical mechanics of Beltrami flows in axisymmetric geometry: Equilibria and bifurcations, J. Stat. Mech. (2010) P06019.
[25] B. Qu, W. J. T. Bos, and A. Naso, Direct numerical simulation of axisymmetric turbulence, Phys. Rev. Fluids **2**, 094608 (2017).
[26] B. Qu, A. Naso, and W. J. T. Bos, Cascades of energy and helicity in axisymmetric turbulence, Phys. Rev. Fluids **3**, 014607 (2018).

[27] P. Chen and M. C. Cross, Statistical two-vortex equilibrium and vortex merger, Phys. Rev. E **53**, R3032(R) (1996).

[28] D. G. Dritschel, W. Qi, and J. B. Marston, On the late-time behaviour of a bounded, inviscid two-dimensional Flow, J. Fluid Mech. **783**, 1 (2015).

[29] A. Szeri and P. Holmes, Nonlinear stability of axisymmetric swirling flows, Phil. Trans. R. Soc. Lond. A **326**, 327 (1988).

[30] The standard helicity is the volume integral of $\mathbf{v}\cdot\boldsymbol{\omega}$, but it is strictly conserved only if the normal vorticity component $\hat{\mathbf{n}}\cdot\boldsymbol{\omega}$ vanishes on the domain boundary. This, in general, fails for the axisymmetric geometry, and so one focuses instead on the closely related combination $v_\theta\omega_\theta$, which avoids the boundary term and whose volume integral Eq. (39) is then, in fact, conserved.

[31] Strictly speaking, the $y = r^2/2$ and z coordinates have different units, and a square mesh does not actually make sense. One should instead use an $a_y \times a_z$ rectangular mesh, or first rescale to dimensionless coordinates, e.g., z/h, y/y_{out}. However, the statistical formalism used here relies only on periodicity of the mesh. So, for simplicity, and with a slight abuse of notation, we do not make this distinction here.

[32] Equation (79) is the s-wave ($l = 0$) case of the Coulomb wave equation: see p. 538 of M. Abramovitz and I. A. Stegun, *Handbook of Mathematical Functions* (Dover, New York, 1970). We note a related spectral analysis of poloidal dynamics within a mean field approximation in Ref. [22], but note as well that the equation there is formulated differently. In particular, the radial component reduces to a Bessel function rather than a Coulomb function, the derived modes do not diagonalize the poloidal kinetic energy term Eq. (26), and their eigenvalues are therefore different from the ones entering the free-energy Eq. (76).

[33] Conversely, in the presence of true antiferromagnetic order, which would be expected for divergent coupling, $\gamma < 1$, and even for sufficiently large $\bar{\beta}$ when $\gamma = 1$, the equilibrium average $\langle\bar{\mu}[\sigma(\boldsymbol{\rho})]\rangle$ will display finite differences between microscale neighboring sites. Hence, noting the scaling Eq. (71) of the Laplacian, both sides of Eq. (99) will display divergent neighboring site difference. It follows that ξ displays (divergent) antiferromagnetic order whenever σ does, scaling as $a^{\gamma-2}$. For $\gamma < 1$ this is larger than the $O(1/\sqrt{\bar{\beta}}a)$ fluctuation scale of ξ, which does not make physical sense.

[34] It follows from Eq. (99) that, even in the presence of antiferromagnetic order, one has $\langle\psi_D\rangle \to 0$, though the scaled equilibrium stream function $a^{-\gamma}\langle\psi_D\rangle$ directly tracks the antiferromagnetic structure in $\langle\bar{\mu}[\sigma(\boldsymbol{\rho})]\rangle$. For $\gamma < 1$, this produces divergent microscale circulating velocity, scaling as $a^{\gamma-1}$, hence unphysically infinite kinetic energy.

[35] There is an analogous rescaling of temperature required to obtain nontrivial *point vortex* Euler equilibria [3], again due to the now unbounded vorticity.

[36] More accurately, the homogeneous 2D Ising antiferromagnet, with fixed $J_z(y) \to J_z^0$ (i.e., no dependence on $1/y$), undergoes a phase transition at a temperature $\bar{T}_c(J_z^0)$. If one now allows inhomogeneous $J_z(y) = J_z^0/y$, then at sufficiently high temperature, $\bar{T} > \bar{T}_c(J_z^0/y_{\min})$, the entire domain will be in the disordered phase, while for sufficiently low temperature, $\bar{T} < \bar{T}_c(J_z^0/y_{\max})$, it will be in the antiferromagnetically ordered phase. In between these two temperatures, $\bar{T}_c(y_{\max}) < \bar{T} < \bar{T}_c(y_{\min})$ there will be a phase boundary at radial coordinate $y_c(\bar{T})$ satisfying $\bar{T}_c(y_c) = \bar{T}$, with the system magnetically ordered for $y < y_c(\bar{T})$ and disordered for $y > y_c(\bar{T})$. In the continuum limit, one is also in the adiabatic limit, and $M_{\text{AF}}(\bar{T}, y) = M_{\text{eq}}(\bar{T}y)$ will exactly follow the local equilibrium value of the sublattice magnetization.

[37] A. Renaud, A. Venaille, and F. Bouchet, Equilibrium statistical mechanics and energy partition for the shallow water model, J. Stat. Phys. **163**, 784 (2016).

[38] H. Lamb, *Hydrodynamics*, 6th ed. (Dover Publications, New York, 1932).

[39] G. K. Batchelor, *An Introduction to Fluid Dynamics* (Cambridge University Press, Cambridge, UK, 1967).

[40] P.-H. Chavanis, Dynamical and thermodynamical stability of two-dimensional flows: Variational principles and relaxation equations, Eur. Phys. J. B **70**, 73 (2009).

[41] P.-H. Chavanis, J. Sommeria, and R. Robert, Statistical mechanics of two-dimensional vortices and collisionless stellar systems, Astrophys. J. **471**, 385 (1996).

[42] P.-H. Chavanis "Statistical mechanics of two-dimensional vortices and stellar systems," in *Dynamics and Thermodynamics of Systems with Long-range Interactions*, edited by T. Dauxois, S. Ruffo, E. Arimondo, and M. Wilkens, Lecture Notes in Physics (Springer, Berlin, 2002), Vol. 602.